AIMS Mathematics, 10(5): 12388–12420.
DOI: 10.3934/math.2025560
Received: 21 March 2025
Revised: 14 May 2025
Accepted: 22 May 2025
Published: 27 May 2025

https://www.aimspress.com/journal/Math

Research article

Modeling anomalous diffusion and volatility in the Australian national electricity market using a space-fractional Black-Scholes framework

Doungporn Wiwatanapataphee[1,*], Yong Hong Wu[1], Wannika Sawangtong[2,3,4] and Panumart Sawangtong[3,4,5]

[1] Curtin University, School of Electrical Engineering, Computing and Mathematical Sciences, Perth, Western Australia

[2] Department of Mathematics, Faculty of Science, Mahidol University, Bangkok, Thailand

[3] Research group for fractional calculus theory and applications, Science and Technology Research Institute, King Mongkut's University of Technology North Bangkok, Bangkok, Thailand

[4] Centre of Excellence in Mathematics, MHESI, Bangkok, 10400, Thailand

[5] Department of Mathematics, Faculty of Applied Science, King Mongkut's University of Technology North Bangkok, Bangkok, Thailand

* **Correspondence:** Email: doungporn.wiwatana@postgrad.curtin.edu.au.

Abstract: Extreme volatility, price spikes, and complex nonlinear dynamics are characteristics often shown in the electricity market, particularly the Australian national electricity market (NEM). These attributes are usually driven by supply-demand imbalances, renewable energy integration, and regulatory interventions, which make traditional pricing models, such as the Black-Scholes framework, inadequate for capturing key market behaviors like long-memory effects, heavy tails, and volatility clustering. This study developed and applied a fractional Black-Scholes model that integrated space-fractional derivatives to account for memory effects, anomalous diffusion, and extreme price movements. The proposed model was calibrated using historical NEM data, demonstrating significant improvements in the pricing of electricity options. The results suggested that it effectively captured key market behaviors. Overall, the findings offered valuable insights and provided a more accurate representation of the Australian electricity market's distinct dynamics.

Keywords: fractional Black-Scholes model; Australian national electricity market; electricity price volatility; volatility clustering; derivative pricing; heavy-tailed behavior
Mathematics Subject Classification: 26A33, 91G20

1. Introduction

The national electricity market (NEM) spot price is complex and unpredictable due to many factors. One of the key features of the NEM is its high volatility, with prices often changing significantly over short periods. These changes are made worse by sharp price spikes, which happen when electricity demand suddenly increases or supply is limited, such as during extreme weather events or unexpected outages at power plants [1–3]. A key factor is the imbalance between supply and demand. The exponential growth of renewable energy sources adds complexity, making it harder to maintain a reliable energy supply, especially when generation doesn't match peak demand [4–6]. Regulatory interventions, such as renewable energy policies, price floors and caps, and price thresholds, also play a crucial role in adding complexity to the electricity market. These factors create nonlinear dynamics, where small incidents can have large, unpredictable impacts on energy prices and availability.

Traditional financial models, such as the Black-Scholes framework, have been widely used to model asset prices and evaluate derivative instruments [7]. However, these mild models often fail to capture the unique features of electricity markets, particularly pricing [8]. It is observed that electricity markets exhibit traits such as long memory, heavy tails (increased likelihood of extreme price changes), and volatility clustering (periods of high price variability occurring together) [9–11].

The Australian NEM, in particular, is known for these complex dynamics, where electricity prices can experience sharp and sudden spikes, as seen in Figure 1. The figure illustrates the time series of electricity demand in megawatt-hour (MW) and prices in Australain dollar per megawatt-hour (AUD/MWh) in New South Wales (NSW). While demand remains relatively stable with seasonal variations, price spikes occur intermittently, often surpassing the price threshold of 5,000 AUD/MWh (dashed line). During the 2024 Australian financial year alone, there were 122 occasions across 16 days where the price exceeded 5,000 AUD/MWh, and 36 of them exceeded 15,000 AUD/MWh. As an example, Figure 2 compares the daily electricity demands and the corresponding prices for a normal day (July 5, 2023) and the day with significant price spikes (May 8, 2024). Despite peak demand periods between 6–9 AM and 3–9 PM, we observe typical price behavior on July 5. On the other hand, price spikes clustering can be seen on May 8, though the demand trends on both dates are fairly similar. This demonstrates prolonged volatility caused by a power plant outage early in the morning of May 8 [12], where prices spiked to 16,600 AUD/MWh and elevated again from 3:40 PM to 7:40 PM, reflecting the lingering effects of the disruption. All in all, these features require advanced mathematical tools for more accurate price modeling and derivative valuation.

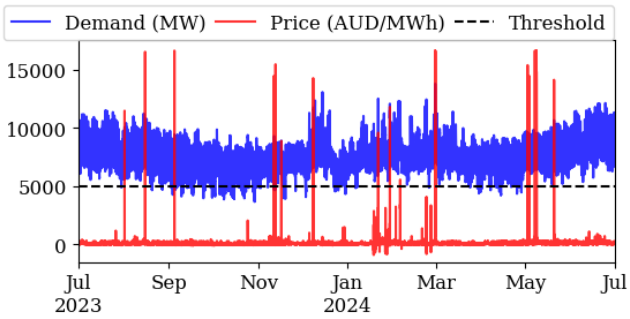

Figure 1. Time series of electricity demand (MW, blue) and price (AUD/MWh, red) during the 2024 Australian financial year for NSW, Australia.

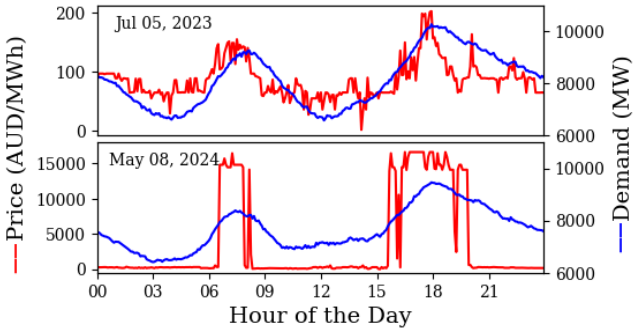

Figure 2. Time series of daily electricity demands (MW, blue) and prices (AUD/MWh, red) for NSW on July 5, 2023 (top) and May 8, 2024 (bottom).

Unlike traditional financial assets, electricity cannot be stored efficiently, leading to supply and demand imbalances that cause sudden and extreme price fluctuations. Figure 3 illustrates the relationship between electricity demands (MW) and spot prices (AUD/MWh) in NSW for the 2024 Australian financial year. While normal prices (green crosses) remain stable across demand levels, price spikes (red circles) occur mostly when demand exceeds 9,000 MW, with extreme events concentrated beyond 10,000 MW. Some price spikes also appear at moderate demand levels, indicating that factors beyond demand, such as generator outages, transmission constraints, or market interventions, contribute to volatility. These dependencies introduce nonlinearity and seasonality into price dynamics, making standard financial models inadequate for capturing the full complexity of energy markets.

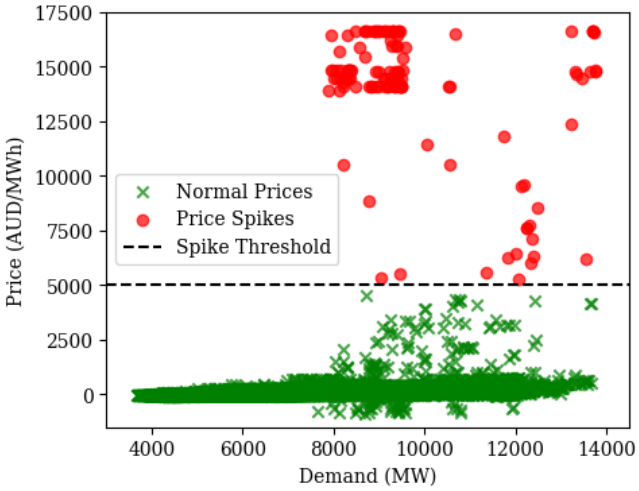

Figure 3. Relationship between electricity prices (AUD/MWh) and demands (MW) in NSW, FY 2024. Normal prices (green crosses) are clustered at lower price levels, while price spikes (red dots) occur at higher price levels.

To tackle the complexities in the electricity market, experts have been looking into new ways to model price behavior, such as mean-reverting processes and jump-diffusion models, with the aim to better capture real-world features like price memory, sudden spikes, and long-term shifts. Researchers have also used stochastic volatility and regime-switching models, which help reflect the varied and often unpredictable nature of electricity prices. The approaches based on fractional calculus have also

gained a lot of attention recently.

The fractional Black-Scholes model represents an enhanced extension of the conventional Black-Scholes framework, incorporating fractional derivatives to better capture the complexities of financial markets. These derivatives account for memory effects and anomalous diffusion, which occur when asset prices deviate from traditional stochastic assumptions [13]. One method involves substituting the standard Brownian motion in the original model with fractional Brownian motion (fBm) to reflect asset price movements with memory effects and long-range dependencies [14–16]. This enhancement provides a more accurate depiction of market behavior, particularly in environments where asset prices exhibit fractal characteristics and volatility clustering [17, 18].

Mathematically, the model incorporates fractional derivatives, which can be defined in various forms, such as Caputo or Riemann-Liouville derivatives [19, 20]. This modification leads to the fractional Black-Scholes framework, which is solved using different numerical and analytical techniques, including finite difference methods, homotopy perturbation approaches, and wavelet-based solutions [21–24]. These methods are essential for deriving practical solutions, especially for pricing European options and other financial derivatives in the presence of fractional volatility and transaction costs [25, 26].

The model's applications extend to multiple areas in financial engineering. It has been used to analyze arbitrage opportunities and replication strategies in complete markets, showing that arbitrage can arise under certain conditions due to its non-semimartingale properties [14, 15, 18]. Additionally, it has been utilized for pricing intricate financial instruments, including double barrier options and chooser options, where traditional models may fall short [17, 27, 28]. The adaptability of the fractional Black-Scholes model makes it a valuable tool for risk management and derivative pricing, particularly in markets exhibiting irregularities and non-standard trends [16, 29–32].

In this paper, we explore how the fractional Black-Scholes model can be applied to the Australian energy market, using fractional calculus to better capture the complex behavior of price movements and improve the pricing of derivatives. Our proposed model builds on the mild Black-Scholes framework by adding space-fractional derivatives, jump processes, and stochastic volatility, allowing for a more accurate representation of the patterns seen in electricity markets and financial assets. To make the complex fractional derivatives easier to handle, we use the generalized Mellin transform, which simplifies them into basic algebraic expressions and makes the model much more tractable. The model effectively addresses several key challenges specific to energy markets, including volatility clustering, price spikes, and non-Gaussian behavior.

The structure of this paper is organized to provide a comprehensive analysis and modeling framework for electricity spot price and option pricing using advanced mathematical techniques. Following the Introduction, Section 2 offers a data analysis of electricity spot prices and option prices to set the empirical context. Section 3 introduces the mathematical formulation, starting with the classic mild Black-Scholes model and advancing to the derivation of a fractional Black-Scholes model incorporating jumps and stochastic volatility. This section also develops a space-fractional extension and applies Mellin transformation techniques to construct a transform-based approach for Put option pricing, with a breakdown of the fractional differential equation components under both constant and stochastic volatility settings. Section 4 is dedicated to model calibration, covering data specification and the calibration procedure to align the model with empirical data. Section 5 presents numerical examples comparing model outcomes under different volatility and jump conditions. Section 6

provides the conclusion, which summarizes the findings and implications of the study.

2. Data analysis of the electricity spot price and options price

This section presents an exploratory data analysis of electricity spot prices and option prices. The historical spot price and demand data for NSW, covering the 2024 financial year from July 1, 2023 to June 30, 2024, was obtained from the Australian Energy Market Operator (AEMO) [33]. Additionally, the corresponding options data was sourced from the Australian and New Zealand Power Market, also known as ASX Energy [34].

The NEM spot prices are determined by the AEMO based on real-time supply and demand. It reflects prices at which electricity is bought and sold in the market at any given moment [35]. On the other hand, electricity options traded on the ASX Energy market allow market participants to hedge against the price volatility in the spot market. These options give buyers the right, but not the obligation, to purchase or sell electricity at a predetermined price within a specific time frame [34]. The spot prices play a key role in pricing electricity options since these financial contracts are directly tied to the value of the underlying spot market. When spot prices are volatile, the premiums for options tend to increase as market participants seek to manage their risk. In the context of this study, the spot price and option price data are employed to estimate the key parameters of the Black-Scholes model. The spot price data helps determine the underlying asset price and historical volatility, while the option price data is used for model calibration.

First, we investigate the characteristics of the electricity spot price data. Figure 4 illustrates spot price volatility clustering across hours of the day and different dates. The color intensity represents different volatility levels, where the red area indicates a high-volatility period, and the blue area represents a low-volatility. As expected in the electricity market, the volatility is concentrated during business hours (8 AM - 4 PM) in most seasons except in the summer period (December to February) and at the beginning of the winter period (June), where they have wider high-volatility bands than others. These higher intraday fluctuations are due to an increase in energy demand.

The distributional analysis of generalized autoregressive conditional heteroskedasticity (GARCH) standardized residuals provides strong evidence of heavy-tailed distribution, as indicated by the extremely high kurtosis (172.99) and the Jarque-Bera test (p-value = 0.0). A normal distribution typically has a kurtosis of 3, but the observed value suggests an excessive concentration of small fluctuations around the mean and a significantly higher probability of extreme price movements. The Jarque-Bera test strongly rejects normality, confirming that the residuals exhibit non-Gaussian characteristics. This is further illustrated in Figure 5(a), which shows a sharp peak at zero alongside fat tails. This indicates that extreme returns occur more frequently than a normal distribution would predict. The quantile-quantile (Q-Q) plot in Figure 5(b) supports this conclusion, as the residuals deviate significantly from the normal reference line at both tails, confirming the presence of large, unpredictable price spikes. These findings have crucial implications for risk modeling, as traditional Gaussian-based models underestimate the probability of extreme market fluctuations, potentially leading to the mispricing of risk.

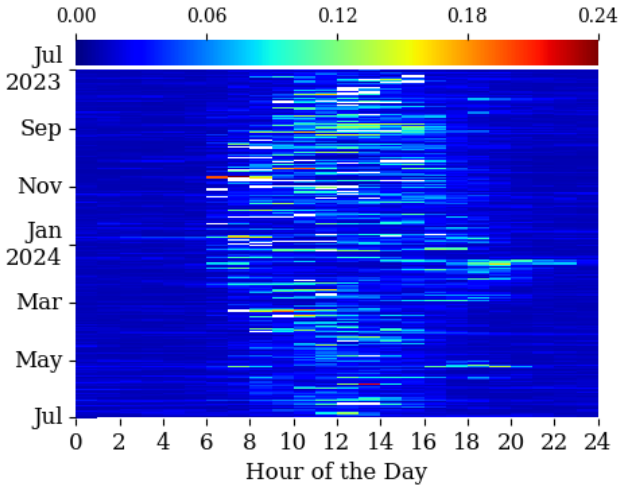

Figure 4. Heatmap showing electricity price volatility across different hours of the day and dates throughout the 2024 financial year in the NEM. The color scale represents the magnitude of price fluctuations, with blue indicating low volatility and red indicating high volatility.

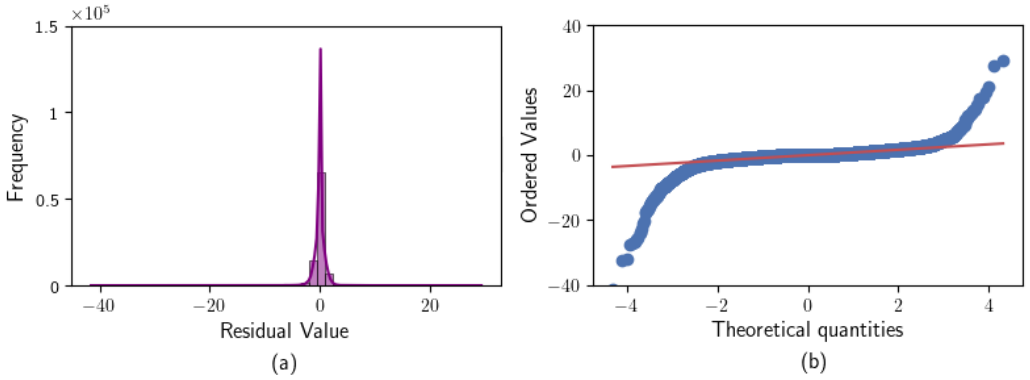

Figure 5. Distribution analysis of GARCH standardized residuals: (a) Histogram of residuals, (b) Q-Q plot versus normal distribution.

Figure 6 illustrates the price progression of the ASX electricity option over time. Call options exhibit a wider range of prices, occasionally reaching higher values, while Put options are more clustered at lower price levels. The clustering of data points in a certain time period indicates higher trading frequency on specific days. Apart from that, the overall trend does not seem to be strongly directional. It shows a considerable fluctuation in option prices without a clear long-term upward or downward movement, indicating market volatility. Some spikes are also observed, suggesting significant trading activity or market shifts at a certain time.

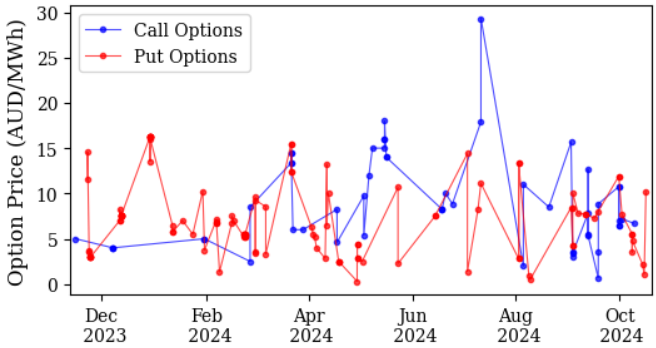

Figure 6. Time series of Call (blue) and Put (red) option prices for ASX electricity contracts from December 2023 to October 2024.

The histogram of ASX electricity option prices, shown in Figure 7, reveals a right-skewed distribution, indicating that most options are priced at the lower end of the scale, with a gradual decline in frequency as prices increase. The majority of transactions appear to be concentrated in the range of 0 to 20 AUD/MWh, suggesting that lower-priced options are more commonly traded. As prices rise, the number of occurrences decreases, though a few higher-priced options still appear as outliers. The price distribution for Put options appears to be more concentrated at lower values, with fewer high-priced contracts compared to Call options.

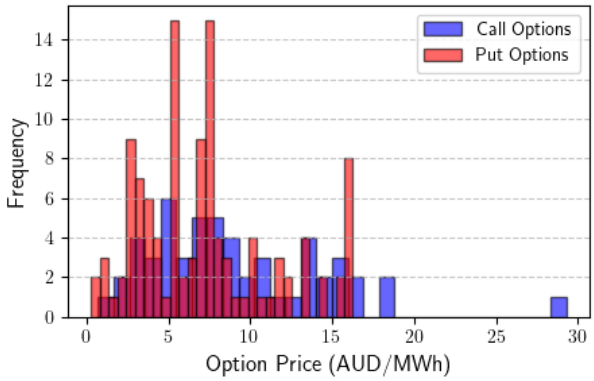

Figure 7. Histogram comparing the price distribution of Call (blue) and Put (red) options for ASX Electricity contracts.

To further investigate the distribution, as well as the connection between strike prices, times to maturity, and option prices, Figure 8 illustrates their relationships in the form of a three-dimensional surface plot. The fitted surface (color gradient) provides an approximation of how option prices evolve based on the strike price and time to maturity, while the red dots indicate actual observed data points. We can see that option prices tend to increase as strike prices rise, particularly for options with shorter time to maturity. The highest peaks (red/yellow regions) suggest periods where option prices spiked, potentially due to market volatility or demand fluctuations. In addition, the uneven surface with fluctuations suggests that electricity option pricing is highly volatile and does not always follow a smooth trend.

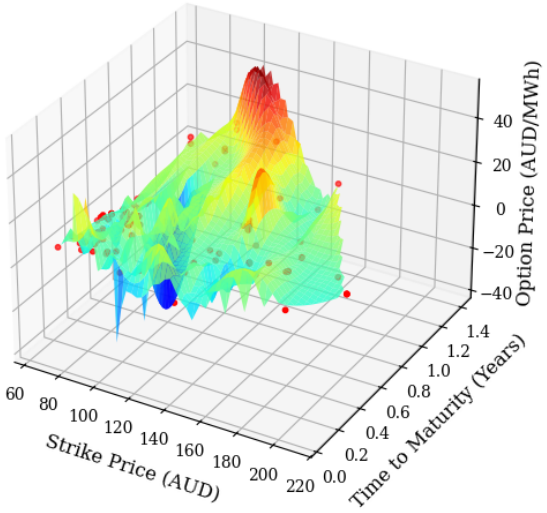

Figure 8. Surface plot of ASX option prices against strike prices and time to maturity.

3. Mathematical formulation

The fractional Black-Scholes model enhances the traditional Black-Scholes framework by integrating fractional derivatives, allowing it to capture memory effects, heavy-tailed distributions, and anomalous diffusion in asset price movements. This section presents the mathematical formulation for the model, focusing on its application to the Australian electricity market.

3.1. Mild Black-Scholes model

The mild Black-Scholes partial differential equation for the option price $u(t, x)$ is

$$\frac{\partial u}{\partial t} + \frac{1}{2}\sigma^2 x^2 \frac{\partial^2 u}{\partial x^2} + rx\frac{\partial u}{\partial x} - ru = 0, \tag{3.1}$$

where t and x denote, respectively, time to expiration (percentage per annum) and the underlying electricity price per share, r is a risk-free interest rate (percentage per annum), and σ^2 is volatility (percentage per annum).

For European call and put options, the following terminal and boundary conditions apply.

i) **Terminal Condition** (at maturity T)

$$u(T, x) = \max\{\pm(x - K), 0\},$$

where the plus sign corresponds to a Call option, the minus sign corresponds to a Put option, and K represents the strike price per share.

ii) **Boundary Conditions**
For a Call option, we have

$$u(t, x) = \begin{cases} 0, & \text{for low stock price,} \\ x, & \text{for high stock price.} \end{cases}$$

For a Put option, we obtain

$$u(t,x) = \begin{cases} Ke^{-r(T-t)}, & \text{for low stock price,} \\ 0, & \text{for high stock price.} \end{cases}$$

3.2. Derivation of the fractional Black-Scholes model with jumps and stochastic volatility

In this section, we derive the extended Black-Scholes model that forms the basis of our framework. This model incorporates fractional diffusion, jump processes, and stochastic volatility to more accurately capture the complex behaviors observed in electricity and energy markets. These enhancements allow the model to reflect key empirical phenomena such as long-range dependence, sudden price discontinuities, and volatility clustering [36, 37].

Under the classical Black-Scholes hypotheses, the spot price x_t evolves as a geometric Brownian motion,

$$dx_t = \mu x_t\, dt + \sigma x_t\, dW_t,$$

where μ is the asset's drift rate, σ its volatility, and W_t a standard Wiener process. Under the assumptions of no-arbitrage and risk-neutral valuation, this leads to the well-known Black-Scholes partial differential equation (PDE) for the option price $u(t, x)$.

However, this mild model fails to account for several important features of high-volatility markets, particularly electricity markets. Specifically, it does not capture heavy-tailed return distributions, jump behavior, or memory effects [36, 38]. To address these limitations, we generalize the model by incorporating the following three key components.

(1) **Fractional Diffusion**

To represent anomalous diffusion and memory effects, we replace the mild second-order spatial derivative with space-fractional derivatives of non-integer orders $\alpha \in (0, 1]$ and $\beta = 1 + \alpha$. In particular, we employ the generalized Caputo derivative, which is better suited for modeling initial value problems and capturing nonlocal dependencies in the asset price dynamics [39, 40].

Furthermore, a scaling parameter $\rho > 0$ is introduced via the conformable derivative, allowing for flexible modeling of asset behavior across different scaling regimes [40].

This modification transforms the mild diffusion term into

$$\left(\frac{x^\rho}{\rho}\right)^\alpha \mathcal{D}_x^{\rho,\alpha} u + \frac{1}{2}\sigma_t^2 \left(\frac{x^\rho}{\rho}\right)^\beta \mathcal{D}_x^{\rho,\beta} u,$$

where $\mathcal{D}_x^{\rho,\beta}$ denotes the generalized Caputo derivative of order β. This formulation captures both the fractal structure and long-memory characteristics present in electricity price movements [38].

(2) **Lévy Jump Processes**

To account for abrupt and significant price changes, we model the asset price as being influenced by Lévy jump-diffusion dynamics [41, 42]. The resulting stochastic differential equation is given by

$$dx_t = \mu x_t\, dt + \sigma_t x_t\, dW_t + x_{t^-}(J-1)\, dN_t,$$

where J represents the random jump size, N_t is a Poisson process with intensity λ, and σ_t is the (possibly stochastic) volatility process.

The infinitesimal generator of this process contributes a nonlocal integral term to the pricing PDE,

$$-\lambda \left(\mathbb{E}[u(t, xJ)] - u(t, x) \right),$$

which captures the expected change in option value due to jump-induced discontinuities in the asset price [42].

(3) **Stochastic Volatility**
We incorporate stochastic volatility to capture the time-varying, state-dependent nature of market uncertainty, recognizing that the real-world financial markets, particularly in the energy sector, experience evolving and clustered volatility during periods of stress or regime change [37].
By allowing volatility σ_t to follow its own stochastic process, the model more accurately represents the dynamics of observed asset returns. This leads to greater realism and improves the model's ability to capture risk patterns, volatility persistence, and market shocks, thereby enhancing pricing accuracy.

Combining these components, the resulting fractional PDE for the option price $u(t, x)$ is

$$\frac{\partial u}{\partial t} + r\left(\frac{x^\rho}{\rho}\right)^\alpha \mathcal{D}_x^{\rho,\alpha} u + \frac{1}{2}\sigma_t^2 \left(\frac{x^\rho}{\rho}\right)^{1+\alpha} \mathcal{D}_x^{\rho,1+\alpha} u - ru = -\lambda \left(\mathbb{E}[u(t, xJ)] - u(t, x) \right), \tag{3.2}$$

subject to the appropriate terminal condition depending on the option type.

This generalized model preserves the no-arbitrage structure of the mild Black-Scholes framework while introducing the necessary flexibility to model real market dynamics in electricity pricing. It is especially suitable for derivative pricing where empirical features such as spikes, clustering, and fat tails are present.

3.3. Space-fractional Black-Scholes equation with jumps and stochastic volatility for Put option prices

To more accurately capture the complex dynamics of financial assets, particularly in electricity markets, Eq (3.2) incorporates space-fractional derivatives, jump processes, and stochastic volatility. This formulation allows the model to reflect key empirical phenomena such as nonlocal memory effects, abrupt price jumps, and volatility clustering, which are not adequately addressed by mild models.

3.3.1. Generalized model formulation

The generalized model employs a generalized Caputo fractional derivative to reflect memory and long-range dependence. This derivative is well-suited to initial value problems, retains physical interpretability, and aligns with mild calculus. In contrast to Riemann-Liouville, Riesz, and traditional Caputo forms, the generalized Caputo derivative offers improved numerical stability and calibration flexibility [38].

The complete space-fractional Black-Scholes equation with jumps and stochastic volatility for the

European Put option price $u(t, x)$ is formulated as follows.

$$\begin{cases} \dfrac{\partial u}{\partial t} + r\left(\dfrac{x^\rho}{\rho}\right)^\alpha \mathcal{D}_x^{\rho,\alpha} u + \dfrac{1}{2}\sigma_t^2 \left(\dfrac{x^\rho}{\rho}\right)^{1+\alpha} \mathcal{D}_x^{\rho,1+\alpha} u - ru = -\lambda\left(\mathbb{E}[u(t, xJ)] - u(t, x)\right), \\ u(T, x) = \begin{cases} \max\left\{\dfrac{K^\rho}{\rho} - \dfrac{x^\rho}{\rho},\ 0\right\}, & \text{if } x \le K, \\ 0, & \text{otherwise.} \end{cases} \end{cases} \tag{3.3}$$

This generalized model retains the no-arbitrage structure of the mild Black-Scholes framework while introducing the necessary flexibility to capture complex market behaviors. By incorporating fractional diffusion, jump dynamics, and stochastic volatility, the model effectively accounts for key empirical features such as fat-tailed return distributions, volatility clustering, and non-Markovian effects, which are commonly observed in electricity and other high-volatility markets but inadequately addressed by traditional models.

3.3.2. Fractional derivative definition

In equation (3.2), $\mathcal{D}_x^{\rho,\beta} u$ denotes the generalized Caputo fractional derivative of order β [38], defined by

$$\mathcal{D}_x^{\rho,\beta} u = \Gamma^{-1}(n-\beta) \int_0^x \left(\frac{x^\rho}{\rho} - \frac{\xi^\rho}{\rho}\right)^{-(1+n+\beta)} \left[\left(T_\xi^\rho\right)^n u(\xi)\right] \frac{d\xi}{\xi^{1-\rho}}, \tag{3.4}$$

where $\rho > 0$ is a scaling parameter, $T_\xi^\rho u(\xi) = \xi^{1-\rho}\dfrac{du}{d\xi}$ is the conformable derivative of order ρ, and $n = \lceil \beta \rceil$ is the smallest integer greater than or equal to β, ensuring $n - 1 < \beta \le n$. The operator $\left(T_\xi^\rho\right)^n u(\xi)$ denotes the n-fold application of the conformable derivative.

For more on the theoretical foundation and motivations behind the generalized Caputo and conformable derivatives used here, we refer the reader to Caputo and Fabrizio [39] and Losada and Nieto [40], who introduced these generalizations to address shortcomings in mild formulations and support more flexible modeling in applied problems.

3.3.3. Stochastic volatility and jump process specifications

The volatility follows a stochastic process governed by the Heston dynamics, which is given by

$$d\sigma_t^2 = \kappa(\theta - \sigma_{t-1}^2)dt + \xi\, dW_t, \tag{3.5}$$

where κ denotes the rate of mean reversion, θ is the long-term variance, ξ represents the volatility of variance process, and W_t is a Wiener process. In Eq (3.2), λ represents the Poisson jump intensity, and J denotes the magnitude of the random jump, which follows a log-normal distribution

$$J \sim \exp(\mu_J + \sigma_J Z), \quad Z \sim \mathcal{N}(0, 1), \tag{3.6}$$

where μ_J and σ_J denote a jump log-mean and a jump log-volatility, respectively. Finally, $\mathbb{E}[u(t, xJ)]$ represents the expectation taken over the jump distribution.

3.4. Existence and uniqueness of solutions

Before proceeding, we must be sure that the fractional Black-Scholes system in (3.3) is well-posed. To that end, we state below the principal results guaranteeing both the existence and uniqueness of mild solutions.

Theorem 1. *(Existence of the Exact Solution) Let $u(t, x)$ satisfy the fractional Black-Scholes equation with jumps and stochastic volatility,*

$$\begin{cases} \dfrac{\partial u}{\partial t} + r\left(\dfrac{x^\rho}{\rho}\right)^\alpha \mathcal{D}_x^{\rho,\alpha} u + \dfrac{1}{2}\sigma_t^2 \left(\dfrac{x^\rho}{\rho}\right)^{1+\alpha} \mathcal{D}_x^{\rho,1+\alpha} u - ru = -\lambda\left(\mathbb{E}[u(t, xJ)] - u(t, x)\right), \\ u(T, x) = \begin{cases} \max\left\{\dfrac{K^\rho}{\rho} - \dfrac{x^\rho}{\rho},\ 0\right\}, & \text{if } x \le K, \\ 0, & \text{otherwise.} \end{cases} \end{cases}$$

Assume the following conditions,

(1) The fractional orders satisfy $0 < \alpha \le 1$, $\beta = 1 + \alpha$, and $\rho > 0$.
(2) The terminal condition $u(T, x) \in C^2((0, \infty)) \cap L^1((0, \infty))$ with at most polynomial growth.
(3) The volatility process σ_t is Lipschitz continuous and bounded on $[0, T]$.
(4) The jump intensity $\lambda > 0$ and the jump size $J \sim \exp(\mu_J + \sigma_J Z)$, with $Z \sim \mathcal{N}(0, 1)$, satisfies $\mathbb{E}[J^2] < \infty$.
(5) The fractional derivatives $\mathcal{D}_x^{\rho,\alpha}$ and $\mathcal{D}_x^{\rho,\beta}$ are defined in the generalized Caputo sense.

Then, there exists a unique mild solution $u(t, x) \in C([0, T]; L^1((0, \infty))) \cap C^{1,2}([0, T] \times (0, \infty))$ to the fractional Black-Scholes equation with jumps and stochastic volatility.

Proof. To establish the existence of a solution, we begin by reformulating the original PDE into an equivalent integral equation. This transformation allows us to leverage fixed-point theory as a powerful analytical tool. To achieve this, we first introduce operator splitting and reformulate the PDE by giving the PDE to be written abstractly as

$$\frac{\partial u}{\partial t} = \mathcal{L}u + \mathcal{J}[u],$$

where $\mathcal{L}u := -r\left(\dfrac{x^\rho}{\rho}\right)^\alpha \mathcal{D}_x^{\rho,\alpha} u - \dfrac{1}{2}\sigma_t^2 \left(\dfrac{x^\rho}{\rho}\right)^{1+\alpha} \mathcal{D}_x^{\rho,1+\alpha} u + ru$, and

$\mathcal{J}[u] := -\lambda\left(\mathbb{E}[u(t, xJ)] - u(t, x)\right)$ is the jump operator, which is linear and nonlocal in space.

We look for a mild solution, i.e., a function $u(t, x)$ satisfying Duhamel's-formula integral equation,

$$u(t, x) = (S_{T-t}\phi)(x) + \left(\int_t^T S_{\tau - t} \mathcal{J}[u(\tau)]\, d\tau\right)(x),$$

where S_t is the semigroup generated by the spatial operator $\mathcal{L}$, and $\phi(x) = u(T, x)$ is the terminal condition.

We now show that the fractional diffusion operator $\mathcal{L}$ indeed produces a strongly continuous analytic semigroup on an appropriate Banach space, which is a key step in constructing the mild solution to the equation.

Based on the theory of fractional powers of sectorial operators (see Kilbas et al., 2006 [43]; Zacher, 2005 [44]), they prove that $\{S_t\}_{t\geq 0}$ extends analytically on spaces like $L^1 \cap C^0((0,\infty))$, provided the hypotheses below are met:

(1) the function u lies in the domain of $\mathcal{L}$, with $\mathrm{Dom}(\mathcal{L}) \subseteq C^2((0,\infty))$;
(2) the fractional operators $\mathcal{D}_x^{\rho,\beta}$ are well-defined on functions that possess sufficient smoothness and decay at infinity, as is typical for financial payoff functions; and
(3) the coefficients r and σ_t are smooth and uniformly bounded over the domain.

Under these assumptions, the homogeneous part of the PDE admits a well-defined mild solution expressed as

$$u_{\mathrm{hom}}(t,x) = (S_{T-t}\phi)(x),$$

where $\phi(x)$ denotes the terminal payoff function.
We then address the jump term by showing that the associated integral operator is bounded and linear in the chosen function space, allowing it to be incorporated into the solution framework via standard fixed-point arguments.

The jump term $\mathcal{J}[u]$ is a bounded linear operator in L^1, assuming that $\mathbb{E}[|J|^2] < \infty$ and $u \in L^1 \cap C^0$. Specifically,

$$\|\mathcal{J}[u](t,\cdot)\|_{L^1} \leq 2\lambda \|u(t,\cdot)\|_{L^1}.$$

This allows us to apply Banach's fixed-point theorem to the integral equation,

$$\mathcal{T}[u(t)](x) := (S_{T-t}\phi)(x) + \left(\int_t^T S_{\tau-t}\mathcal{J}[u(\tau)]d\tau\right)(x),$$

where $\mathcal{T}$ is a contraction mapping on the Banach space $C([0,T]; L^1((0,\infty)))$ for small enough time intervals or suitably small λ.

Finally, we apply the Banach fixed-point theorem to the problem's integral formulation, ensuring the existence of a unique mild solution within the chosen function space. By verifying that

(1) $\mathcal{T}$ maps a closed convex subset into itself, and
(2) $\mathcal{T}$ is a contraction under the norm, $\|u\|_\omega := \sup_{t\in[0,T]} e^{\omega t}\|u(t)\|_{L^1}$ for some $\omega > 0$,

we conclude that there is a unique mild solution, $u \in C([0,T]; L^1)$, which can be bootstrapped to lie in $C^{1,2}([0,T]\times(0,\infty))$ due to the smoothing attributes of the analytic semigroup S_t.
Thus, under the stated assumptions, a mild solution exists to the fractional Black-Scholes PDE with jumps and stochastic volatility.

□

Theorem 2. *(Uniqueness of the Exact Solution) Assume the same conditions as in Theorem 1; there is a solution $u(t,x)$ satisfying the fractional Black-Scholes PDE with jumps and stochastic volatility is unique in the function space $C^{1,2}([0,T]\times(0,\infty))$.*

Proof. We prove uniqueness by contradiction using the energy method and an adaptation of the maximum principle for fractional differential operators, which has been established for both Caputo and generalized Caputo formulations in the literature.

First, we assume that $u_1(t,x)$ and $u_2(t,x)$ are two solutions to the problem defined in Eq (3.3) with the same initial and boundary conditions, and set

$$w(t,x) := u_1(t,x) - u_2(t,x).$$

Then, w solves the homogeneous version of the PDE,

$$\frac{\partial w}{\partial t} + r\left(\frac{x^\rho}{\rho}\right)^\alpha \mathcal{D}_x^{\rho,\alpha} w + \frac{1}{2}\sigma_t^2 \left(\frac{x^\rho}{\rho}\right)^{1+\alpha} \mathcal{D}_x^{\rho,1+\alpha} w - rw = -\lambda\left(\mathbb{E}[w(t,xJ)] - w(t,x)\right),$$

subject to the terminal condition $w(T,x) = 0$. Multiplying both sides by $w(t,x)$ and integrating over the domain $(0,\infty)$ yields

$$\int_0^\infty w\frac{\partial w}{\partial t}\,dx + r\int_0^\infty w\left(\frac{x^\rho}{\rho}\right)^\alpha \mathcal{D}_x^{\rho,\alpha} w\,dx + \frac{1}{2}\int_0^\infty w\,\sigma_t^2\left(\frac{x^\rho}{\rho}\right)^{1+\alpha} \mathcal{D}_x^{\rho,1+\alpha} w\,dx - r\int_0^\infty w^2\,dx$$

$$= -\lambda\int_0^\infty w(t,x)\left(\mathbb{E}[w(t,xJ)] - w(t,x)\right)dx.$$

Next, we analyze each term of the energy identity derived from the difference between the two solutions. The first term simplifies to $\frac{1}{2}\frac{d}{dt}\|w(t,\cdot)\|_{L^2}^2$, representing the time derivative of the squared L^2-norm of the difference function $w(t,x)$. The coercivity of the generalized Caputo derivative, as established in the literature (see Zacher, 2005 [44]; Luchko, 2009 [45]) ensures that the fractional diffusion terms contribute a nonnegative quantity to the energy. On the other hand, the jump-term integral

$$\int_0^\infty w(t,x)\left(\mathbb{E}[w(t,xJ)] - w(t,x)\right)dx$$

follows from Jensen's inequality and the convexity of the L^2-norm, ensuring that the jump component does not contribute positively to the energy estimate.

Finally, we apply Grönwall's inequality to the differential inequality obtained from the previous analysis. Specifically, we have

$$\frac{d}{dt}\|w(t,\cdot)\|_{L^2}^2 \le 0,$$

which implies that the squared L^2-norm of the difference $w(t,x) = u_1(t,x) - u_2(t,x)$ is nonincreasing over time. Given the terminal condition $w(T,x) = 0$, it follows directly that $\|w(t,\cdot)\|_{L^2}^2 = 0$ for all $t \in [0,T]$. Accordingly, $w(t,x) \equiv 0$ for all $(t,x) \in [0,T]\times(0,\infty)$, which proves that the two solutions coincide. Therefore, the fractional Black-Scholes equation admits a unique solution in the function space $C^{1,2}([0,T]\times(0,\infty))$. □

Remark: While the above analysis establishes existence and uniqueness under a set of reasonable assumptions, it is not without limitations. The results rely heavily on the regularity of the terminal payoff, the boundedness and smoothness of model coefficients, and the coercivity of the fractional operators within specific function spaces such as $L^1 \cap C^0$ or $C^{1,2}$. However, in practical settings, especially in electricity markets, the payoff functions and volatility dynamics may not always exhibit the required smoothness or boundedness, and the behavior near boundaries (e.g., $x \to 0$) may be more singular. Moreover, the analysis focuses on mild solutions and does not address the existence of classical solutions in the strong or weak sense under more general initial and boundary conditions.

3.5. Generalized Mellin transformation

Definition. Let $f : [0,\infty) \to \mathfrak{R}$ be a real-valued function. Its generalized Mellin transform and corresponding inversion formula are defined as follows.

$$\widetilde{f}(c) = \mathcal{M}_\rho\left[f(x)\right](c) = \int_0^\infty f(x)\left(\frac{x^\rho}{\rho}\right)^{c-1}\frac{dx}{x^{1-\rho}}, \tag{3.7}$$

$$f(x) = \mathcal{M}_\rho^{-1}\left[\widetilde{f}(c)\right](x) = \frac{1}{2\pi j}\int_{\varepsilon-j\omega}^{\varepsilon+j\omega}\widetilde{f}(c)\left(\frac{x^\rho}{\rho}\right)^{-c} dc, \tag{3.8}$$

where c is the complex parameter of the generalized Mellin transform, $\mathfrak{R}(c) \in \Omega$, the largest open strip in which the integral exists.

Lemma. *Let $f : [0,\infty) \to \mathfrak{R}$ be a real-valued function that is generalized Mellin transformable. Then, for any real constant α and for all c satisfying $\mathfrak{R}(c+\alpha) \in \Omega$, the following shift property holds,*

$$\mathcal{M}_\rho\Big[\Big(\frac{x^\rho}{\rho}\Big)^\alpha f(x)\Big](c) = \widetilde{f}(c+\alpha).$$

Proof. Consider $\mathcal{M}_\rho\Big[(\frac{x^\rho}{\rho})^\alpha f(x)\Big](c) = \int_0^\infty \Big[(\frac{x^\rho}{\rho})^\alpha f(x)\Big](\frac{x^\rho}{\rho})^{c-1}\ \frac{dx}{x^{1-\rho}}$.

Observe that $(\frac{x^\rho}{\rho})^{c-1}(\frac{x^\rho}{\rho})^\alpha = (\frac{x^\rho}{\rho})^{c-1+\alpha} = (\frac{x^\rho}{\rho})^{(c+\alpha)-1}$. Hence, the integral becomes

$$\int_0^\infty (\tfrac{x^\rho}{\rho})^{(c+\alpha)-1} f(x)\,\frac{dx}{x^{1-\rho}}.$$

By the definition of the generalized Mellin transform, the above integral is

$$\int_0^\infty (\tfrac{x^\rho}{\rho})^{(c+\alpha)-1} f(x)\,\frac{dx}{x^{1-\rho}} = \widetilde{f}(c+\alpha).$$

Therefore, we have shown that

$$\mathcal{M}_\rho\Big[(\tfrac{x^\rho}{\rho})^\alpha f(x)\Big](c) = \widetilde{f}(c+\alpha),$$

which completes the proof of the lemma. □

Theorem 3. *Let $f : [0,\infty) \to \mathfrak{R}$ be a real-valued function and let α be a real number satisfying $0 < \alpha \le 1$. Suppose that f is the generalized Mellin transformable. Then, for all c (with $\mathfrak{R}(c)$ in the appropriate strip Ω), the following identity holds.*

$$\mathcal{M}_\rho\left[\left(\frac{x^\rho}{\rho}\right)^\alpha D_x^{\rho,\alpha} f(x)\right](c) = -\frac{c\,\Gamma(-c)}{\rho\,\Gamma(1-\alpha-c)}\,\widetilde{f}(c),$$

where $\widetilde{f}(c)$ denotes the generalized Mellin transform of f.

Proof. For a function $f(x)$, the generalized Mellin transform is defined by

$$\widetilde{f}(c) = \int_0^\infty \left(\frac{x^\rho}{\rho}\right)^{c-1} f(x)\,\frac{dx}{x^{1-\rho}},$$

and its inversion is given (when it exists) by

$$f(x) = \frac{1}{2\pi j}\int_{\varepsilon-j\infty}^{\varepsilon+j\infty} \left(\frac{x^\rho}{\rho}\right)^{-c} \widetilde{f}(c)\,dc$$

with ε chosen so that the vertical line $\Re(c) = \varepsilon$ lies within the fundamental strip Ω. For $0 < \alpha \leq 1$, the generalized Caputo derivative of f is defined as

$$D_x^{\rho,\,\alpha} f(x) = \frac{1}{\Gamma(1-\alpha)}\int_0^x \left(\frac{x^\rho}{\rho} - \frac{\xi^\rho}{\rho}\right)^{-\alpha} T_\xi^\rho f(\xi)\,\frac{d\xi}{\xi^{1-\rho}},$$

where the conformable derivative T_ξ^ρ (see Khalil et al., 2014 [46]) is given by

$$T_\xi^\rho f(\xi) = \xi^{1-\rho}\frac{d}{d\xi} f(\xi).$$

We now compute

$$\mathcal{M}_\rho\left[\left(\frac{x^\rho}{\rho}\right)^\alpha D_x^{\rho,\alpha} f(x)\right](c) = \int_0^\infty \left(\frac{x^\rho}{\rho}\right)^{c-1}\left(\frac{x^\rho}{\rho}\right)^\alpha D_x^{\rho,\alpha} f(x)\frac{dx}{x^{1-\rho}},$$

and show that it equals

$$-\frac{c\,\Gamma(-c)}{\rho\,\Gamma(1-\alpha-c)}\,\widetilde{f}(c).$$

Notice that

$$\left(\frac{x^\rho}{\rho}\right)^{c-1}\left(\frac{x^\rho}{\rho}\right)^\alpha = \left(\frac{x^\rho}{\rho}\right)^{-(1-\alpha-c)} = \left(\frac{x^\rho}{\rho}\right)^{(c+\alpha)-1}.$$

By definition,

$$\mathcal{M}_\rho\left[\left(\frac{x^\rho}{\rho}\right)^\alpha D_x^{\rho,\alpha} f(x)\right](c) = \Gamma^{-1}(1-\alpha)\int_0^\infty \left(\frac{x^\rho}{\rho}\right)^{-(1-\alpha-c)}\left[\int_0^x \left(\frac{x^\rho}{\rho} - \frac{\xi^\rho}{\rho}\right)^{-\alpha} T_\xi^\rho f(\xi)\,\frac{d\xi}{\xi^{1-\rho}}\right]\frac{dx}{x^{1-\rho}}.$$

Assuming that we can exchange the order of integration (which is justified if f and its derivatives decay appropriately), we write

$$\mathcal{M}_\rho\left[\left(\frac{x^\rho}{\rho}\right)^\alpha D_x^{\rho,\alpha} f(x)\right](c) = \frac{1}{\Gamma(1-\alpha)}\int_0^\infty T_\xi^\rho f(\xi)\left[\int_\xi^\infty \left(\frac{x^\rho}{\rho}\right)^{-(1-\alpha-c)}\left(\frac{x^\rho}{\rho} - \frac{\xi^\rho}{\rho}\right)^{-\alpha}\frac{dx}{x^{1-\rho}}\right]\frac{d\xi}{\xi^{1-\rho}}.$$

Let us denote the inner integral by $I(c,\xi)$, then

$$I(c,\xi) = \int_\xi^\infty \left(\frac{x^\rho}{\rho}\right)^{-(1-\alpha-c)}\left(\frac{x^\rho}{\rho} - \frac{\xi^\rho}{\rho}\right)^{-\alpha}\frac{dx}{x^{1-\rho}}.$$

Introducing the change of variable, we have $u = \frac{x^\rho}{\rho}, \quad w = \frac{\xi^\rho}{\rho}$. Then, it is noted that

$$x = (\rho u)^{1/\rho} \quad \text{and} \quad dx/x^{1-\rho} = \frac{du}{\rho}.$$

Under this change, we have $u = w$ when $x = \xi$, and the inner integral becomes

$$I(c,\xi) = \frac{1}{\rho}\int_w^\infty u^{-(1-\alpha-c)}\,(\,u-w\,)^{-\alpha}\,du.$$

A standard integral formula tells us that for $\Re(c) < 0$ (and with proper conditions on α) we have

$$\int_w^\infty u^{-(1-\alpha-c)}(u-w)^{-\alpha}\,du = w^{c-1}\,\frac{\Gamma(1-\alpha)\,\Gamma(-c)}{\Gamma(1-\alpha-c)}.$$

Thus,

$$I(c,\xi) = \frac{1}{\rho}\,w^{c-1}\,\frac{\Gamma(1-\alpha)\,\Gamma(-c)}{\Gamma(1-\alpha-c)} = \frac{1}{\rho}\left(\frac{\xi^\rho}{\rho}\right)^{c-1}\frac{\Gamma(1-\alpha)\,\Gamma(-c)}{\Gamma(1-\alpha-c)}.$$

Returning to the full transform, we now have

$$\mathcal{M}_\rho\left[\left(\frac{x^\rho}{\rho}\right)^\alpha D_x^{\rho,\alpha} f(x)\right](c) = \frac{\Gamma(-c)}{\rho\,\Gamma(1-\alpha-c)}\int_0^\infty T_\xi^\rho f(\xi)\left(\frac{\xi^\rho}{\rho}\right)^{c-1}\frac{d\xi}{\xi^{1-\rho}}.$$

Considering the conformable derivative defined by $T_\xi^\rho f(\xi) = \xi^{1-\rho}\,f'(\xi)$, and taking its generalized Mellin transform, we have

$$\int_0^\infty T_\xi^\rho f(\xi)\left(\frac{\xi^\rho}{\rho}\right)^{c-1}\frac{d\xi}{\xi^{1-\rho}} = \int_0^\infty \xi^{1-\rho}\,f'(\xi)\left(\frac{\xi^\rho}{\rho}\right)^{c-1}\frac{d\xi}{\xi^{1-\rho}} = \int_0^\infty f'(\xi)\left(\frac{\xi^\rho}{\rho}\right)^{c-1} d\xi,$$

since the factor $\xi^{1-\rho}$ in the definition of $T_\xi^\rho f(\xi)$ cancels with the factor $1/\xi^{1-\rho}$ in the measure. Now, using integration by parts with

$$u = \left(\frac{\xi^\rho}{\rho}\right)^{c-1}, \quad dv = f'(\xi)d\xi, \quad du = (c-1)\left(\frac{\xi^\rho}{\rho}\right)^{c-1}\frac{d\xi}{\xi},$$

and assuming that the boundary terms vanish (which is ensured by the conditions on f), we obtain

$$\int_0^\infty f'(\xi)\left(\frac{\xi^\rho}{\rho}\right)^{c-1} d\xi = -(c-1)\int_0^\infty f(\xi)\left(\frac{\xi^\rho}{\rho}\right)^{c-1}\frac{d\xi}{\xi}.$$

Notice that by the definition of the generalized Mellin transform (with weight $1/\xi^{1-\rho}$), one may show that (see standard properties of the Mellin transform)

$$\int_0^\infty T_\xi^\rho f(\xi)\left(\frac{\xi^\rho}{\rho}\right)^{c-1}\frac{d\xi}{\xi^{1-\rho}} = -c\,\widetilde{f}(c).$$

It is noted that in the mild Mellin transform, the property $\mathcal{M}\Big[xf'(x)\Big](c) = -c\,\widetilde{f}(c)$ holds, and the conformable derivative T_ξ^ρ is designed so that the generalized Mellin transform has an analogous property. Thus, we conclude that

$$\int_0^\infty T_\xi^\rho f(\xi)\left(\frac{\xi^\rho}{\rho}\right)^{c-1}\frac{d\xi}{\xi^{1-\rho}} = -c\,\widetilde{f}(c).$$

Substituting this into the previous expression yields

$$\mathcal{M}_\rho\left[\left(\frac{x^\rho}{\rho}\right)^\alpha \mathcal{D}_x^{\rho,\alpha} f(x)\right](c) = -\frac{c\,\Gamma(-c)}{\rho\,\Gamma(1-\alpha-c)}\widetilde{f}(c).$$

This completes the proof. □

Remark: The choice of the conformable derivative is motivated by its simplicity and compatibility with classical calculus. Unlike traditional definitions of fractional derivatives, the conformable form preserves many desirable properties such as the product, chain, and quotient rules, making it easier to work with in analytical settings. Moreover, its locality and ease of numerical implementation make it particularly suitable for applications in financial modeling, where intuitive interpretation and computational tractability are essential.

Theorem 4. *Let $f : [0,\infty) \to \mathfrak{R}$ be a real-valued function and let β be a real number with $1 < \beta \le 2$. Assume that f is generalized Mellin transformable. Then, for all c with $\mathfrak{R}(c) \in \Omega$, we have*

$$\mathcal{M}_\rho\left[\left(\frac{x^\rho}{\rho}\right)^\beta \mathcal{D}_x^{\rho,\beta} f(x)\right](c) = \frac{1}{\rho}\,\frac{c(c+1)\,\Gamma(-c-1)}{\Gamma(1-c-\beta)}\,\widetilde{f}(c),$$

where $\widetilde{f}(c)$ denotes the generalized Mellin transform of f.

Proof. For a function $f(x)$, the generalized Mellin transform is

$$\widetilde{f}(c) \;=\; \mathcal{M}_\rho[f(x)](c) \;=\; \int_0^\infty \left(\tfrac{x^\rho}{\rho}\right)^{c-1} f(x)\,\frac{dx}{x^{1-\rho}},$$

valid for $\mathfrak{R}(c)$ in some fundamental strip Ω. For generalized Caputo derivative $\mathcal{D}_x^{\rho,\beta}$ with $1 < \beta \le 2$, by definition (for $n = 2$, since $1 < \beta \le 2$ implies $n - \beta = 2 - \beta$),

$$D_x^{\rho,\beta} f(x) \;=\; \frac{1}{\Gamma(2-\beta)}\int_0^x \left(\tfrac{x^\rho}{\rho} - \tfrac{\xi^\rho}{\rho}\right)^{1-\beta-1} (T_\xi^\rho)^2 f(\xi)\,\frac{d\xi}{\xi^{1-\rho}},$$

where $(T_x^\rho)^2$ is the second conformable derivative operator (i.e., apply T_x^ρ twice), and

$$T_x^\rho f(x) = x^{1-\rho}\,\frac{d}{dx}[f(x)].$$

Since $1 - \beta - 1 = -\beta$, we rewrite

$$D_x^{\rho,\beta} f(x) \;=\; \frac{1}{\Gamma(2-\beta)}\int_0^x \left(\tfrac{x^\rho}{\rho} - \tfrac{\xi^\rho}{\rho}\right)^{-\beta} (T_\xi^\rho)^2 f(\xi)\,\frac{d\xi}{\xi^{1-\rho}}.$$

We want to show

$$\mathcal{M}_\rho\Big[\Big(\tfrac{x^\rho}{\rho}\Big)^\beta D_x^{\rho,\beta} f(x)\Big](c) = \frac{1}{\rho}\frac{c(c+1)\,\Gamma(-c-1)}{\Gamma(1-\beta-c)}\,\widetilde{f}(c).$$

Considering the transform

$$\mathcal{M}_\rho\Big[\Big(\tfrac{x^\rho}{\rho}\Big)^\beta D_x^{\rho,\beta} f(x)\Big](c) = \int_0^\infty \Big(\tfrac{x^\rho}{\rho}\Big)^{c-1}\Big(\tfrac{x^\rho}{\rho}\Big)^\beta D_x^{\rho,\beta} f(x)\,\frac{dx}{x^{1-\rho}} = \int_0^\infty \Big(\tfrac{x^\rho}{\rho}\Big)^{(c+\beta)-1} D_x^{\rho,\beta} f(x)\,\frac{dx}{x^{1-\rho}},$$

and using

$$D_x^{\rho,\beta} f(x) = \frac{1}{\Gamma(2-\beta)}\int_0^x \Big(\tfrac{x^\rho}{\rho} - \tfrac{\xi^\rho}{\rho}\Big)^{-\beta}(T_\xi^\rho)^2 f(\xi)\,\frac{d\xi}{\xi^{1-\rho}},$$

we get

$$\begin{aligned}\mathcal{M}_\rho\Big[\Big(\tfrac{x^\rho}{\rho}\Big)^\beta D_x^{\rho,\beta} f(x)\Big](c) &= \frac{1}{\Gamma(2-\beta)}\int_0^\infty \Big(\tfrac{x^\rho}{\rho}\Big)^{(c+\beta)-1}\left[\int_0^x \Big(\tfrac{x^\rho}{\rho} - \tfrac{\xi^\rho}{\rho}\Big)^{-\beta}(T_\xi^\rho)^2 f(\xi)\,\frac{d\xi}{\xi^{1-\rho}}\right]\frac{dx}{x^{1-\rho}} \\ &= \frac{1}{\Gamma(2-\beta)}\int_0^\infty (T_\xi^\rho)^2 f(\xi)\,\frac{d\xi}{\xi^{1-\rho}}\int_\xi^\infty \Big(\tfrac{x^\rho}{\rho}\Big)^{(c+\beta)-1}\Big(\tfrac{x^\rho}{\rho} - \tfrac{\xi^\rho}{\rho}\Big)^{-\beta}\frac{dx}{x^{1-\rho}}.\end{aligned}$$

Denote the inner x-integral by $\mathcal{I}(c,\xi)$, such that

$$\mathcal{I}(c,\xi) = \int_\xi^\infty \Big(\tfrac{x^\rho}{\rho}\Big)^{(c+\beta)-1}\Big(\tfrac{x^\rho}{\rho} - \tfrac{\xi^\rho}{\rho}\Big)^{-\beta}\frac{dx}{x^{1-\rho}}.$$

Substitute $u = \frac{x^\rho}{\rho}$ and $w = \frac{\xi^\rho}{\rho}$. Then,

$$x = (\rho u)^{1/\rho}, \quad dx = \frac{1}{\rho}(\rho u)^{\frac{1}{\rho}-1}\,du, \quad \frac{dx}{x^{1-\rho}} = \frac{du}{\rho}.$$

When $x = \xi$, we have

$$\mathcal{I}(c,\xi) = \rho^{-1}\int_w^\infty u^{-(1-\beta-c)}\,(u-w)^{-\beta}\,du.$$

If $\Re(c) < -\beta$ or so, then the standard Beta function identity yields

$$\int_w^\infty u^{c+\beta-1}\,(u-w)^{-\beta}\,du = w^{c-1}\,\Gamma(2-\beta)\,\frac{\Gamma(-c-1)}{\Gamma(1-\beta-c)}.$$

Thus,

$$\mathcal{I}(c,\xi) = \frac{1}{\rho}\,w^{c-1}\,\Gamma(2-\beta)\,\frac{\Gamma(-c-1)}{\Gamma(1-\beta-c)} = \frac{1}{\rho}\Big(\tfrac{\xi^\rho}{\rho}\Big)^{c-1}\Gamma(2-\beta)\,\frac{\Gamma(-c-1)}{\Gamma(1-\beta-c)}.$$

We have

$$\begin{aligned}\mathcal{M}_\rho\Big[\Big(\tfrac{x^\rho}{\rho}\Big)^\beta D_x^{\rho,\beta} f\Big](c) &= \frac{1}{\Gamma(2-\beta)}\int_0^\infty (T_\xi^\rho)^2 f(\xi)\,\frac{d\xi}{\xi^{1-\rho}}\Big[\frac{1}{\rho}\,\Gamma(2-\beta)\Big(\tfrac{\xi^\rho}{\rho}\Big)^{c-1}\,\frac{\Gamma(-c-1)}{\Gamma(1-\beta-c)}\Big] \\ &= \frac{1}{\rho}\,\frac{\Gamma(-c-1)}{\Gamma(1-\beta-c)}\int_0^\infty (T_\xi^\rho)^2 f(\xi)\Big(\tfrac{\xi^\rho}{\rho}\Big)^{c-1}\frac{d\xi}{\xi^{1-\rho}}.\end{aligned}$$

We now consider the term $(T_{\xi}^{\rho})^2 f(\xi)$. As $T_{\xi}^{\rho} f(\xi) = \xi^{1-\rho} \frac{d}{d\xi} f(\xi)$, we get $(T_{\xi}^{\rho})^2 f(\xi) = T_{\xi}^{\rho}\Big(\xi^{1-\rho} f'(\xi)\Big)$. One can show that in the Mellin domain, applying $(T_x^{\rho})^2$ to f corresponds to multiplying the transform by $c(c+1)$. Concretely,

$$\mathcal{M}_{\rho}\Big[(T_x^{\rho})^2 f(x)\Big](c) = c(c+1)\,\widetilde{f}(c),$$

which can be seen as an analogue of the mild Mellin property. Hence,

$$\int_0^{\infty} (T_{\xi}^{\rho})^2 f(\xi) \left(\frac{\xi^{\rho}}{\rho}\right)^{c-1} \frac{d\xi}{\xi^{1-\rho}} = c(c+1)\,\widetilde{f}(c).$$

Thus,

$$\mathcal{M}_{\rho}\Big[\Big(\frac{x^{\rho}}{\rho}\Big)^{\beta} D_x^{\rho,\beta} f(x)\Big](c) = \frac{1}{\rho}\,\frac{c(c+1)\Gamma(-c-1)}{\Gamma(1-\beta-c)}\,\widetilde{f}(c).$$

for $\Re(c) \in \Omega$. Hence, the theorem is proved.

□

3.6. A transform-based approach for Put option pricing analysis

To solve the system (3.3), we apply the generalized Mellin transform to each term of Eq $(3.3)_1$ and terminal condition $(3.3)_2$.

1. Time derivative

Since the transform is with respect to x only, we have

$$\mathcal{M}_{\rho}\left\{\frac{\partial u}{\partial t}\right\}(t,c) = \frac{\partial \widetilde{u}(t,c)}{\partial t}.$$

2. First fractional term $\mathcal{F}_1$ with constant r

For $\mathcal{F}_1 \equiv r\left(\frac{x^{\rho}}{\rho}\right)^{\alpha} \mathcal{D}_x^{\rho,\alpha} u(x,t)$, using **Theorem 3** as $0 < \alpha \leq 1$, one has

$$\mathcal{M}_{\rho}\Big[\mathcal{F}_1\Big](c) = -rA(c)\,\widetilde{u}(t,c),$$

where $A(c) = \dfrac{1}{\rho}\dfrac{c\,\Gamma(-c)}{\Gamma(1-\alpha-c)}$ for $\Re(c)$ in the fundamental strip.

3. Second fractional term $\mathcal{F}_2$

i. For constant volatility, we set $\mathcal{F}_2 \equiv \frac{\sigma^2}{2}\left(\frac{x^{\rho}}{\rho}\right)^{1+\alpha} D_x^{\rho,1+\alpha} u$, and using **Theorem 4** as $1 < 1+\alpha \leq 2$, one has

$$\mathcal{M}_{\rho}\Big[\mathcal{F}_2\Big](c) = \frac{\sigma^2}{2}\,B(c)\,\widetilde{u}(t,c),$$

where $B(c) = \dfrac{1}{\rho}\dfrac{c(c+1)\,\Gamma(-c-1)}{\Gamma(-\alpha-c)}$ for $\Re(c)$ in the fundamental strip.

ii. Stochastic volatility

With the Heston model, the constant $\frac{\sigma^2}{2}B(c)$ is replaced by

$$\ln M\left(t, \sigma_t^2; \frac{1}{2}B(c)\right) = \ln \mathbb{E}\left[e^{\frac{1}{2}B(c)\int_t^T \sigma_\tau^2 \, d\tau}\right],$$

which is the *log* of the PDE/Monte Carlo solution for the integrated variance transform. Hence,

$$\mathcal{M}_\rho\left[\mathcal{F}_2\right](c) = \ln\left(\mathbb{E}\left[e^{\frac{1}{2}B(c)\int_t^T \sigma_\tau^2 \, d\tau}\right]\right)\widetilde{u}(t, c).$$

4. The $-r\,u(t, x)$ term

This term transforms directly to $\mathcal{M}_\rho\left[-r\,u(t, x)\right](c) = -r\,\widetilde{u}(t, c)$.

5. The jump term $\mathcal{J}$

For the jump term $\mathcal{J} \equiv -\lambda\Big(\mathbb{E}[u(t, xJ)] - u(t, x)\Big)$, we apply the shift property (**Lemma**) to note that

$$\mathcal{M}_\rho\Big[\mathbb{E}[u(t, xJ)]\Big] = \mathbb{E}[J^{-\rho c}]\,\tilde{u}(t, c),$$

where $\mathbb{E}[J^{-\rho c}]$ is the moment generating function of the jump distribution. Thus,

$$\mathcal{M}_\rho\left\{\mathcal{J}\right\}(c) = -\lambda\Big(e^{C(\rho,c)} - 1\Big)\widetilde{u}(t, c), \quad \text{with} \quad C(\rho, c) = -\rho c\mu_J + \frac{1}{2}\rho^2 c^2 \sigma_J^2.$$

6. Terminal condition

$$u(T, x) = \begin{cases} \dfrac{K^\rho}{\rho} - \dfrac{x^\rho}{\rho}, & x \le K, \\ 0, & \text{oterwise.} \end{cases}$$

Thus,

$$\begin{aligned} \widetilde{u}(T, c) = \int_0^\infty \left(\frac{x^\rho}{\rho}\right)^{c-1} u(T, x)\frac{dx}{x^{1-\rho}} &= \int_0^K \left(\frac{x^\rho}{\rho}\right)^{c-1}\left(\frac{K^\rho}{\rho} - \frac{x^\rho}{\rho}\right)\frac{dx}{x^{1-\rho}} \\ &= \frac{1}{\rho^{c-1}}\int_0^K x^{\rho c-1}\left(\frac{K^\rho}{\rho} - \frac{x^\rho}{\rho}\right)dx. \end{aligned}$$

Factoring out the common factor $1/\rho$,

$$\widetilde{u}(T, c) = \frac{1}{\rho^c}\int_0^K x^{\rho c-1}\left(K^\rho - x^\rho\right)dx$$

and splitting the integral yield

$$\widetilde{u}(T, c) = \frac{1}{\rho^c}\left[K^\rho \int_0^K x^{\rho c-1}\,dx - \int_0^K x^{\rho c-1}x^\rho\,dx\right].$$

Since $x^{\rho c-1}x^{\rho} = x^{\rho(c+1)-1}$, the integrals become standard power-law integrals.
Recall that for $\Re(\gamma) > 0$, $\int_0^K x^{\gamma-1}\,dx = \frac{K^{\gamma}}{\gamma}$. For the first integral, letting $\gamma = \rho c$ gives

$$\int_0^K x^{\rho c-1}\,dx = \frac{K^{\rho c}}{\rho c}.$$

For the second integral, letting $\gamma = \rho(c+1)$ provides

$$\int_0^K x^{\rho(c+1)-1}\,dx = \frac{K^{\rho(c+1)}}{\rho(c+1)}.$$

Substituting these results, we obtain the terminal condition (payoff) given in Mellin space,

$$\widetilde{u}(T,c) = \frac{1}{\rho^c}\left[K^{\rho}\cdot\frac{K^{\rho c}}{\rho c} - \frac{K^{\rho(c+1)}}{\rho(c+1)}\right] = \frac{K^{\rho(c+1)}}{\rho^{c+1}}\left[\frac{1}{c} - \frac{1}{c+1}\right] = \frac{K^{\rho(c+1)}}{\rho^{c+1}\,c(c+1)}.$$

3.6.1. Generalized Mellin formulation with constant volatility

Substituting these above terms in case of constant volatility into the transformed equation gives

$$\frac{d\tilde{u}(t,c)}{dt} + p(c)\,\tilde{u}(t,c) = 0, \tag{3.9}$$

with the solution

$$\tilde{u}(t,c) = \tilde{u}(T,c)e^{-p(c)(T-t)}, \tag{3.10}$$

where $p(c) = r\,(A(c)+1) - \frac{1}{2}\sigma^2\,B(c) - \lambda\Big(\mathbb{E}[J^{-\rho c}] - 1\Big)$. By using the inversion of the generalized Mellin transform to reconstruct the option price, we have

$$u(t,x) = \frac{1}{2\pi j}\int_{\varepsilon-j\omega}^{\varepsilon+j\omega}\left(\frac{x^{\rho}}{\rho}\right)^{-c}\tilde{u}(T,c)e^{-p(c)(T-t)}\,dc, \quad \text{with } \omega \in [-\omega_{max}, \omega_{max}]. \tag{3.11}$$

3.6.2. Generalized Mellin formulation with stochastic volatility

By substituting these above terms in case of stochastic volatility into the transformed equation and solving the ordinary differential equation, we obtain the Mellin-transformed solution

$$\widetilde{u}(t,c) = \widetilde{u}(T,c)\,e^{-\left[r(A(c)+1)+\lambda\left(e^{C(\rho,c)}-1\right)\right](T-t)}e^{\ln M\left(t,\sigma_t;\frac{1}{2}B(c)\right)}.$$

Finally, $u(t,x)$ is recovered via the inverse generalized Mellin transform (3.11).

4. Model calibration

There are several main steps and considerations to calibrate the fractional Black-Scholes model to historical Put option prices.

4.1. Data collection and model specification

Historical put option prices, $u_{\text{market,i}}$, and corresponding strike prices and time to maturities observed at different dates across the 2024 financial year were gathered from ASX Energy [34]. In addition, the underlying asset prices x_t were obtained from the AEMO NEM [33]. After data cleaning and preparation, the resulting data frame features are shown in Table 1.

Table 1. Historical option price data features and description.

Feature	Unit	Description
Code		Asset code
Date		Date and time in Australian Eastern Daylight Time (AEDT)
Underlying	AUD/MWh	Underlying asset price taken from AEMO spot price
Strike	AUD	Strike price of the asset
TimeToMaturity	Year	Time to maturity of the asset
OptionPrice	AUD/MWh	Option price taken from ASX electricity options
OptionType		Option type: 'P' for Put and 'C' for Call

The goal is to find parameters θ, which include (i) fractional exponent $\alpha \in (0, 1]$ for the first derivative, (ii) scale factor ρ, (iii) volatility σ, (iv) jump parameters $(\lambda, \mu_J, \sigma_J)$, and any additional terms for stochastic volatility, such that the model's theoretical prices match the historical data as closely as possible. We denote this set of parameters collectively by θ. Then, the model produces a theoretical put price, $u_{\text{model,i}}(\theta)$, for each strike-maturity pair.

4.2. Calibration procedure

After collecting the data and specifying the fractional model with its parameters θ, the following tasks are carried out.

i. The fractional PDE is solved for the theoretical price $u_{\text{model},i}$ for each data point i.

ii. The objective function is to minimize four error metrics, namely, the sum of squared error (SSE), mean absolute error (MAE), mean squared error (MSE), and mean absolute percentage error (MAPE), of $\Delta u_i(\theta) = u_{\text{model},i}(\theta) - u_{\text{market},i}$, and is defined by

$$\min_{\theta} J(\theta) = \mathbf{w}^T \mathbf{C}(\theta), \tag{4.1}$$

where $\mathbf{w}^T = \begin{bmatrix} \delta & \zeta & \xi & \psi \end{bmatrix}$, $\mathbf{C}^T(\theta) = \begin{bmatrix} \text{SSE}(\theta) & \text{MAE}(\theta) & \text{MSE}(\theta) & \text{MAPE}(\theta) \end{bmatrix}$,

with
$$\text{SSE}(\theta) = \sum_{i\in\{1,\ldots,N\}} \Big[\Delta u_i(\theta)\Big]^2, \qquad \text{MAE}(\theta) = \frac{1}{N} \sum_{i\in\{1,\ldots,N\}} \Big|\Delta u_i(\theta)\Big|,$$
$$\text{MSE}(\theta) = \frac{\text{SSE}(\theta)}{N}, \qquad \text{MAPE}(\theta) = \frac{100}{N} \sum_{i\in\{1,\ldots,N\}} \left|\frac{\Delta u_i(\theta)}{u_{\text{market},i}}\right|,$$

and the coefficients δ, ζ, ξ, and ψ are nonnegative weighting factors that determine the relative importance of each error metric in calibrating the parameter θ.

iii. The objective over θ is to minimize using differential evolutions.

iv. The resulting parameters are validated.

Alternatively, the model calibration can be performed according to the Algorithm 1.

Algorithm 1 Calibrate Fractional Option Pricing Model*

Input: Historical option data, initial guess $v_0 = [\alpha_0, \rho_0]$, bounds = $[\alpha, \rho]$, fixed model parameters.
Output: Calibrated parameters $[\alpha^*, \rho^*]$.
procedure CALIBRATION
    Load data features: Date, Underlying, Strike, TimeToMaturity, OptionPrice, OptionType.
    Perform an 80-20 split to create training and test (validation) datasets.
    Training Phase:
    for each Monte Carlo simulation **do**
        Compute integrated variance using Euler-Maruyama method.
    end for
    Compute Laplace transform of the integrated variance using the log-sum-exp trick for numerical stability.
    Define $\tilde{U}(s,t)$ using fractional derivative eigenvalue factors and jump component.
    Define $u(x,t)$ as the inverse generalized Mellin transform of $\tilde{U}(s,t)$.
    Formulate the objective function based on the Eq (4.1).
    Estimate the objective function's gradient using finite differences.
    Set up the IPOPT optimization problem with decision variables $[\alpha, \rho]$, initial guess x_0, and prescribed bounds.
    Configure IPOPT options (e.g., tolerance levels, maximum number of iterations, verbosity).
    Solve the IPOPT problem to minimize the objective function.
    Validation Phase:
    Using the optimized parameters $[\alpha^*, \rho^*]$, compute option prices for the test set.
    Calculate validation error.
    Return the optimized parameters $[\alpha^*, \rho^*]$, validation error, and computation time.
end procedure

5. Numerical examples

In the following analysis, we apply the fractional Black-Scholes Model to analyze electricity price and option dynamics using historical data. This analysis illustrates the model's ability to capture complex price dynamics, including volatility clustering and extreme price spikes, and evaluates its implications for option pricing. For comparison purposes, the numerical examples of the fractional model with constant volatility are presented together with stochastic volatility and jumps.

Here, we consider the effects of scaling parameter ρ and fractional order α on put option prices under the fractional Black-Sholes with different volatility and jump patterns using model parameters as shown in Table 2.

*IPOPT (Interior Point OPTimizer) is an open-source software package for large-scale nonlinear optimization of constrained problems. It is designed to find local solutions using a primal-dual interior-point approach. See Wächter and Biegler (2006), Mathematical Programming, 106(1), 25–57.

Table 2. Model parameters used for analyzing the effects of the scaling parameter ρ and fractional order α on Put option prices.

Variable	Value	Description
r	0.05	Risk-free interest rate
σ	0.2	Constant volatility
σ_0	0.004	Initial volatility
λ	0.1	Jump intensity
μ_J	-0.1	Jump log-mean
σ_J	0.2	Jump log-volatility
θ	0.04	Long-term mean of variance
κ	1.5	Mean reversion rate
η	0.03	Volatility of variance
T	1.0	Maturity time
K	100	Strike price parameter
ϵ	0.02	Real part of c for the Bromwich contour
ω_{max}	8	Imaginary range

5.1. Fractional Black-Scholes model with constant volatility

Figure 9 presents three-dimensional surfaces of the Put option prices under the fractional Black-Scholes framework with constant volatility for a fixed fractional order $\alpha = 0.8$ but different scaling parameter ρ of 0.5 and 1.0. In both figures, the horizontal axes represent the asset price x and time t, while the vertical axis and color gradient indicate the computed Put option prices. Figure 9(a) shows the option-pricing surface when $\rho = 0.5$, while Figure 9(b) shows the surface under $\rho = 1.0$.

Figure 10 examines how the Put option prices under the constant volatility model depend on the scale factor ρ (Figure 10(a)) and the fractional orders α (Figure 10(b)). This can be investigated by plotting the computed Put option prices u against the asset prices x. While fixing the value of α to 0.8, each curve in Figure 10(a) corresponds to a value of $\rho \in \{0.5, 0.8, 1.0\}$. It is observed that as ρ varies, the entire shape of the Put-price profile shifts. Generally, the price is higher for smaller x and lower for larger x. Changing the parameter ρ alters how quickly the price drops as x increases. In the fractional Black-Scholes model, ρ scales how x^ρ influences the PDE. Larger or smaller values of ρ can significantly change the spread of prices, reflecting a different weighting of the underlying effect in the fractional derivative term.

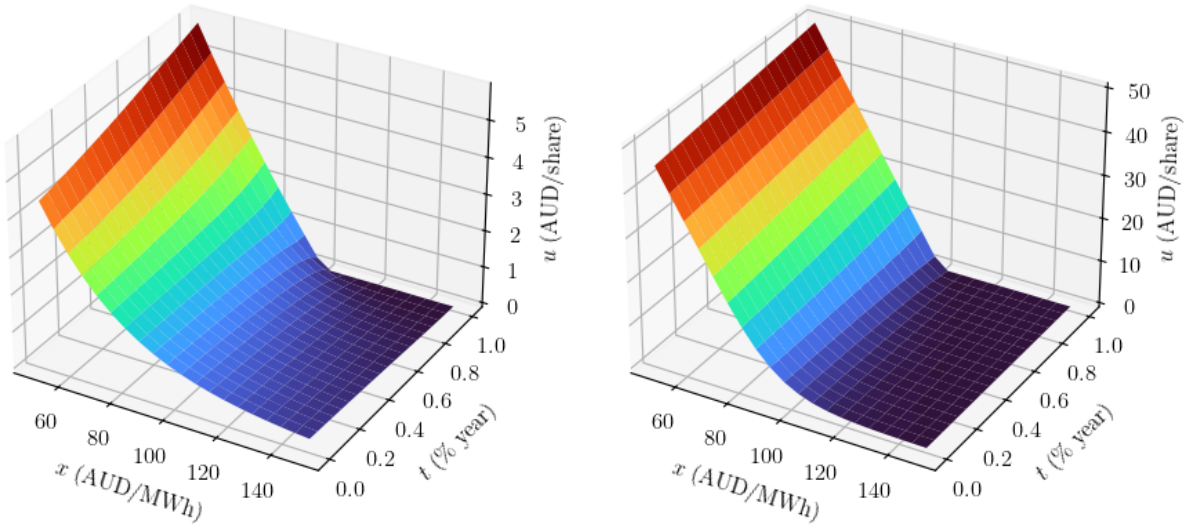

(a) $\rho = 0.5$ (b) $\rho = 1.0$

Figure 9. Surface plots of Put option price obtained from the fractional Black-Scholes model with constant volatility of 0.2, fractional orders $\alpha = 0.8$, and different factor scales: (a) $\rho = 0.5$; (b) $\rho = 1.0$.

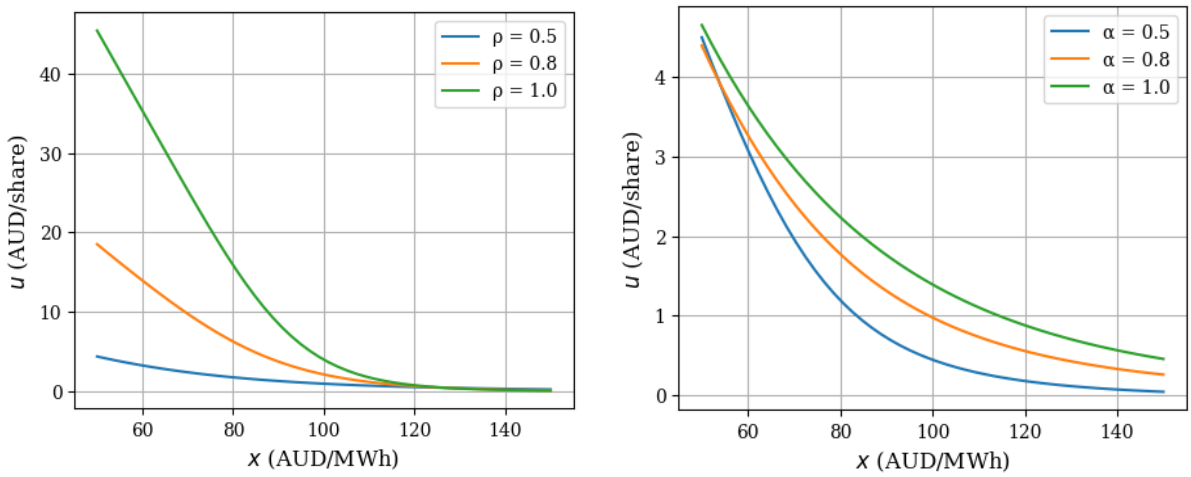

(a) Effect of ρ with $\alpha = 0.8$ (b) Effect of α with $\rho = 0.5$

Figure 10. Put option price profiles obtained from the fractional Black-Scholes model with constant volatility of 0.2 under the various values of (a) scaling parameter ρ with $\alpha = 0.8$; (b) fractional order α with $\rho = 0.5$.

Likewise, each curve in Figure 10(b) corresponds to a value of $\alpha \in \{0.5, 0.8, 1.0\}$. Here, the value of ρ is fixed to 0.5. Varying α changes how the fractional derivative behaves. As α moves from lower to higher values, the slope and magnitude of the Put-price curve shift. In many cases, increasing α makes the fractional PDE behave more like the mild ($\alpha = 1$) Black-Scholes equation, whereas smaller α tends to amplify or dampen certain regions of the price curve. The fractional order α controls how strongly memory or nonlocal effects appear in the pricing model. Noticeably, a lower α produces a different shape compared to the standard ($\alpha = 1$) Black-Scholes result.

Thus, we can conclude that in the fractional Black-Sholes model with constant volatility and no jump component, the Put option prices decrease as x grows (consistent with a standard put payoff shape), but the rate and level of that decrease are strongly influenced by the scale factor ρ and the fractional order α. Smaller ρ or smaller α can shift the entire curve upward or downward and alter how rapidly the price decays with x. This highlights the flexibility of the fractional Black–Scholes model in capturing various market dynamics beyond the mild ($\rho = 1$, $\alpha = 1$) case.

5.2. *Fractional Black-Scholes model with stochastic volatility and jumps*

In comparison to the previous section, the three-dimensional surface plots of the Put option prices under the fractional Black-Scholes model with stochastic volatility and jumps for a fractional order $\alpha = 0.8$ are presented for scaling parameter ρ of 0.5 and 1.0 in Figure 11 (a) and (b), respectively. The plots retain the same axes structure: asset prices x and time t on the horizontal axes, while the vertical axis and color gradient represent the computed Put option prices u.

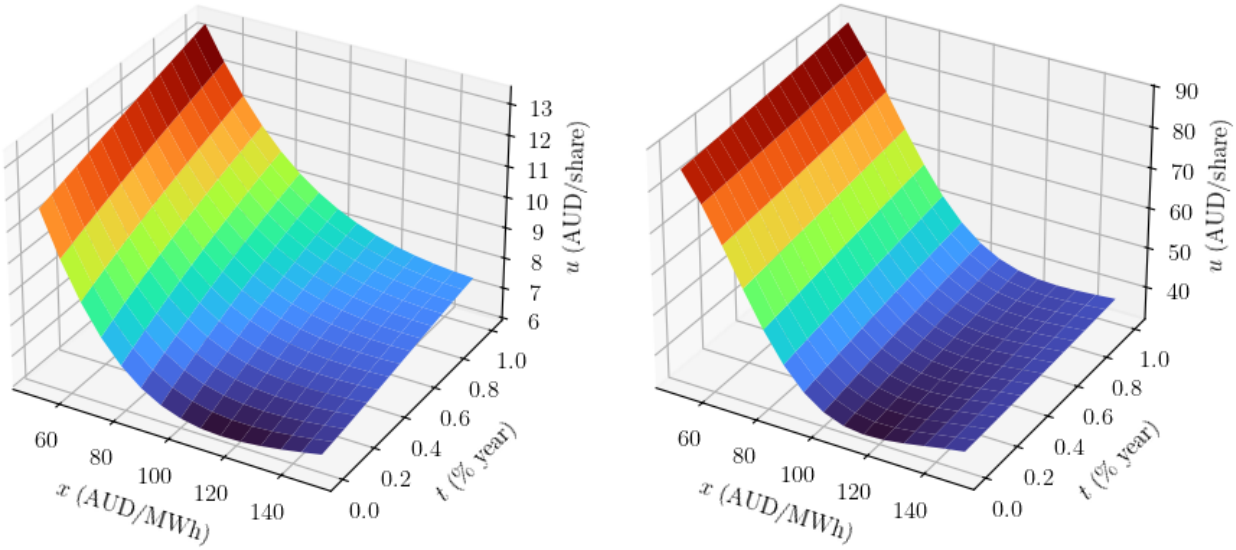

(a) $\rho = 0.5$ (b) $\rho = 1.0$

Figure 11. Surface plots of Put option prices obtained from the fractional Black-Scholes model with stochastic volatility, fractional orders $\alpha = 0.8$, and different scaling parameters: (a) $\rho = 0.5$; (b) $\rho = 1.0$.

While the price surfaces follow a similar downward trend as in the constant volatility model, the incorporation of stochastic volatility and jumps results in slightly higher Put option prices, particularly for lower asset prices (x) and shorter maturities (t). Additionally, the pricing surfaces appear smoother, as the inclusion of stochastic volatility mitigates sharp variations that might otherwise occur. This effect is particularly noticeable near $t = 1.0$, where the price changes gradually.

The impact of the scaling parameter ρ and the fractional order α on Put option prices is further explored in Figure 12. In Figure 12(a), the Put option prices are plotted against asset prices x for different values of ρ while keeping $\alpha = 0.8$ fixed. A key observation is that higher values of ρ result in higher Put option prices, which is more obvious compared to the constant volatility case. Again,

Figure 12(b) examines the effect of α on option prices when $\rho = 0.5$, showing that increasing α again shifts the price curve closer to that of the mild Black-Scholes model.

Overall, the results indicate that introducing stochastic volatility and jumps leads to higher put option prices compared to the constant volatility case. This is particularly evident when considering shorter maturities and lower asset prices. The inclusion of these features allows for a richer representation of real market dynamics, where price fluctuations and jumps play a significant role.

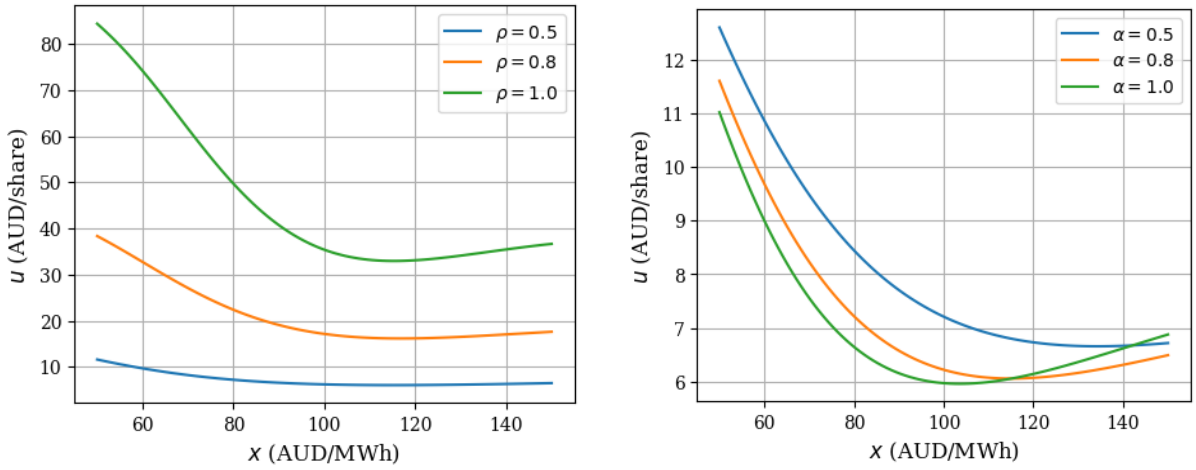

(a) Effect of ρ with $\alpha = 0.8$ (b) Effect of α with $\rho = 0.5$

Figure 12. Profiles of Put option prices $u(T, x)$ obtained from the fractional Black-Scholes model with stochastic volatility and jump component under the various values of (a) scaling parameter ρ with $\alpha = 0.8$; (b) fractional order α with $\rho = 0.5$.

5.3. Model calibration results

To accurately estimate the parameters of the modified fractional Black-Scholes model, we employ a calibration process stated in Section 4 to optimally determine the fractional order α and the scaling parameter ρ.

First, we define the decision variable vector as $v = [\alpha, \rho]$ and set the initial guess ($v_0 = [\alpha_0, \rho_0]$), lower bound ($v_{lb} = [\alpha_{lb}, \rho_{lb}]$), and upper bounds ($v_{ub} = [\alpha_{up}, \rho_{ub}]$) to $[0.5, 0.5]$, $[0.01, 0.01]$, and $[1.0, 1.0]$, respectively. Then, the calibration is performed according to the Algorithm 1 using an optimization based on the Interior Point Optimizer (IPOPT) via the `cyipopt` package, which seeks to minimize errors between observed market prices and model-generated option prices. The optimization is conducted iteratively by simulating volatility dynamics using a Monte Carlo approach and computing option prices via a generalized Mellin transform method. After convergence, the optimal parameter estimates $[\alpha^*, \rho^*]$ are obtained as $[0.1, 0.3457]$. A low fractional order α implies that the second-order market effect is very small, and the market moves are almost entirely in the form of jumps or big moves.

Lastly, we investigate the effectiveness of the calibration by comparing the market Put option prices with the computed Put option prices based on the standard Black-Scholes model and the modified fractional Black-Scholes model. The outcomes displayed in Figure 13 and Table 3 demonstrate that the modified fractional Black-Scholes model yields markedly improved estimates for Put option prices

relative to the classical model. In Figure 13, the modified model (red crosses) aligns more closely with market prices (blue circles) than the standard model (green crosses), particularly in the range of strike prices where deviations are evident in the standard model. This improvement is quantitatively supported by the training and test error metrics in Table 3. In addition to the MSE for each model, the root mean squared error (RMSE) was also calculated. The modified model drastically reduces all the error metrics. These reductions suggest that the modified fractional model captures market behavior with much higher precision, making it a more effective approach for option pricing in the electricity market. In addition, the significantly lower error values indicate that the modified fractional Black-Scholes model provides a better fit to market prices, likely due to its ability to account for volatility and jumps, which are absent in the traditional Black-Scholes framework.

Table 3. Summary of error metrics (SSE, MAE, MSE, RMSE, MAPE) comparing the traditional Black-Scholes model and the modified fractional Black-Scholes model.

	Traditional Model		**Modified Model**	
	Train	**Test**	**Train**	**Test**
SSE	16329.0843	37970.3435	36.7883	120.4764
MAE	15.4683	17.2276	0.8564	1.6216
MSE	480.2672	558.3874	1.0820	3.5434
RMSE	21.9150	23.6302	1.0402	1.8824
MAPE	222.6019	408.8288	15.3877	25.8946

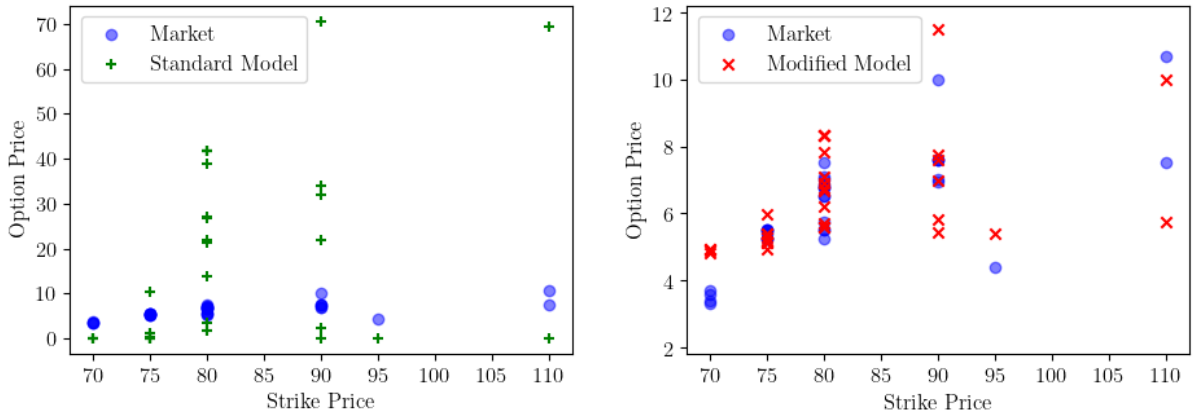

(a) Standard Black-Scholes Model (b) Modified Fractional Black-Scholes Model

Figure 13. Comparison of market Put option prices (blue circles) with (a) the standard Black-Scholes model (green crosses) and (b) the modified fractional Black-Scholes model (red crosses) across varying strike prices.

6. Conclusions

This study demonstrates the effectiveness of fractional Black-Scholes models in addressing the limitations of mild models for electricity option pricing, particularly in capturing memory effects, volatility clustering, and heavy-tailed price dynamics. Using historical demand and spot price data

from the AEMO between July 1 2023 and June 30 2024, the analysis reveals significant improvements in modeling accuracy and market realism.

The modified model, which incorporates stochastic volatility and jump processes, successfully captures upward and downward price spikes as well as volatility clustering observed in real market data. This results in more realistic option prices, especially for lower stock prices and shorter maturity times. In comparison, the standard model produces smooth price behavior but fails to account for extreme price movements and volatility clustering.

In summary, the fractional Black-Scholes framework presented in this study offers a robust and realistic approach for modeling electricity option prices. By incorporating stochastic volatility, jumps, and fractional derivatives, the modified model addresses the limitations of traditional methods. It provides an improved representation of price dynamics, risk measures, and derivative valuations, making it particularly suitable for capturing the unique characteristics of complex and volatile energy markets.

Author contributions

D. Wiwatanapataphee: Conceptualization, investigation, software, formal analysis, visualization, writing - original draft; W. Sawangtong and P. Sawangtong: Methodology, validation; D. Wiwatanapataphee and Y. H. Wu: Writing - review & editing; Y. H. Wu, W. Sawangtong and P. Sawangtong: Supervision. All authors have read and approved the final version of the manuscript for publication.

Use of Generative-AI tools declaration

The authors declare they have not used Artificial Intelligence (AI) tools in the creation of this article.

Acknowledgments

This research was funded by National Science, Research and Innovation Fund (NSRF), and King Mongkut's University of Technology North Bangkok with Contract no. KMUTNB-FF-68-B-38.

Conflict of interest

All authors declare no conflicts of interest in this paper

References

1. C. Conticini, J. A. Filar, A. N. Ganjehlou, A note on price volatility in the Australian electricity market, *ANZIAM J.*, **51** (2009), 730–746. https://doi.org/10.21914/anziamj.v51i0.2655
2. H. Higgs, A. C. Worthington, Systematic features of high-frequency volatility in Australian electricity markets: Intraday patterns, information arrival and calendar effects, *Energy J.*, **26** (2005), 23–42. https://doi.org/10.1007/BF02687427

3. A. C. Worthington, H. Higgs, The impact of generation mix on Australian wholesale electricity prices, *Energ. Source. Part B*, **12** (2017), 223–230. https://doi.org/10.1007/s11377-017-0166-0
4. Y. Alsaedi, G. A. Tularam, V. Wong, Assessing the effects of solar and wind prices on the Australia electricity spot and options markets using a vector autoregression analysis, *Int. J. Energy Econ. Policy*, **10** (2020), 120–133. https://doi.org/10.32479/ijeep.8567
5. S. Goodarzi, H. N. Perera, D. W. Bunn, The impact of renewable energy forecast errors on imbalance volumes and electricity spot prices, *Energy Policy*, **134** (2019), 110827. https://doi.org/10.1016/j.enpol.2019.06.035
6. B. Mountain, Market power and generation from renewables: The case of wind in the south Australian electricity market, *Econ. Energy Env. Pol.*, **2** (2013), 55–72.
7. F. Black, M. Scholes, The pricing of options and corporate liabilities, *J. Polit. Econ.*, **81** (1973), 637–654. https://doi.org/10.1086/260062
8. J. Doran, E. I. Ronn, The bias in Black-Scholes/Black implied volatility: An analysis of equity and energy markets, *Rev. Deriv. Res.*, **8** (2006), 177–198. https://doi.org/10.1007/s11147-006-9002-2
9. J. Elder, A. Serletis, Long memory in energy futures prices, *Rev. Financ. Econ.*, **17** (2007), 146–155. https://doi.org/10.1016/j.rfe.2006.10.002
10. O. Jude, Recent examination of energy markets volatility, *Stud. Bus. Econ.*, **18** (2023), 118–128.
11. F. Paraschiv, R. Hadzi-Mishev, D. Keles, Extreme value theory for heavy tails in electricity prices, *J. Energy Markets*, **9** (2016), 21–50. https://doi.org/10.21314/JEM.2016.141
12. *AER, Reports on Q2 2024 high electricity price events*, 2024, Accessed: 2024-11-30.
13. S. Kumar, D. Kumar, J. Singh, Numerical computation of fractional Black-Scholes equation arising in financial market, *Egypt. J. Basic Appl. Sci.*, **1** (2014), 177–183. https://doi.org/10.1016/j.ejbas.2014.10.003
14. A. Golbabai, O. Nikan, T. Nikazad, Numerical analysis of time fractional Black-Scholes European option pricing model arising in financial market, *Comput. Appl. Math.*, **38** (2019). https://doi.org/10.1007/s40314-019-0957-7
15. X. Wang, Scaling and long-range dependence in option pricing I: pricing European option with transaction costs under the fractional Black-Scholes model, *Physica A*, **389** (2020), 438–444. https://doi.org/10.1016/j.physa.2009.09.041
16. W. Zhao, *Research on fractional option pricing model under real Brownian motion environment*, In: 2009 First International Conference on Information Science and Engineering, IEEE, 2009, 5047–5050. https://doi.org/10.1109/ICISE.2009.954
17. M. Qayyum, E. Ahmad, New solutions of time- and space-fractional Black-Scholes European option pricing model via fractional extension of He-Aboodh algorithm, *J. Math.*, **2024** (2024), 1–19. https://doi.org/10.1155/2024/6623636
18. T. Sottinen, E. Valkeila, On arbitrage and replication in the fractional Black-Scholes pricing model, *Stat. Decis.*, **21** (2003), 93–108. https://doi.org/10.1524/stnd.21.2.93.19003
19. C. Czichowsky, R. Peyre, W. Schachermayer, J. Yang, Shadow prices, fractional Brownian motion, and portfolio optimisation under transaction costs, *Financ. Stoch.*, **22** (2017), 161–180. https://doi.org/10.1007/s00780-017-0351-5

20. P. Sawangtong, K. Trachoo, W. Sawangtong, B. Wiwattanapataphee, The analytical solution for the Black-Scholes equation with two assets in the Liouville-Caputo fractional derivative sense, *Mathematics*, **6** (2018), 129. https://doi.org/10.3390/math6080129
21. R. Jena, S. Chakraverty, A new iterative method based solution for fractional Black-Scholes option pricing equations (BSOPE), *SN Appl. Sci.*, **1** (2018), 95. https://doi.org/10.1007/s42452-018-0106-8
22. L. Song, W. Wang, Solution of the fractional Black-Scholes option pricing model by finite difference method, *Abstr. Appl. Anal.*, **2013** (2013), 1–10. https://doi.org/10.1155/2013/596218
23. A. Sugandha, E. Rusyaman, S. Sukono, E. Carnia, Using a mix of finite difference methods and fractional differential transformations to solve modified Black-Scholes fractional equations, *Mathematics*, **12** (2024),1077. https://doi.org/10.3390/math12071077
24. Y. Sun, W. Gong, H. Dai, L. Yuan, Numerical method for american option pricing under the time-fractional Black-Scholes model, *Math. Probl. Eng.*, **2023** (2023). https://doi.org/10.1155/2023/4669161
25. J. Aguilar, J. Korbel, Simple formulas for pricing and hedging european options in the finite moment log-stable model, *Risks*, **7** (2019), 36. https://doi.org/10.3390/risks7020036
26. D. Prathumwan, K. Trachoo, On the solution of two-dimensional fractional Black-Scholes equation for European put option, *Adv. Differ. Equ.*, **2020** (2020), 146. https://doi.org/10.1186/s13662-020-02554-8
27. H. Kleinert, J. Korbel, Option pricing beyond Black-Scholes based on double-fractional diffusion, *Physica A*, **449** (2016), 200–214. https://doi.org/10.1016/j.physa.2015.12.125
28. L. Song, A semianalytical solution of the fractional derivative model and its application in financial market, *Complexity*, 2018. https://doi.org/10.1155/2018/1872409
29. F. Azevedo, Z. Vale, A. Vale, Hedging using futures and options contracts in the electricity market, *Renew. Energ. Power Qual. J.*, **1** (2003). https://doi.org/10.24084/repqj01.407
30. T. Bjork, H. Hult, A note on wick products and the fractional Black-Scholes model, *Financ. Stoch.*, **9** (2005), 197–209. https://doi.org/10.1007/s00780-004-0144-5
31. S. Liu, Z. Xu, The inverse problem of time-fractional order and volatility for European option under time-fractional Black-Scholes model, *J. Phys. Conf. Ser.*, **2905** (2024). https://doi.org/10.1088/1742-6596/2905/1/012010
32. H. Zhang, M. Zhang, F. Liu, M. Shen, Review of the fractional Black-Scholes equations and their solution techniques, *Fractal Fract.*, **8** (2024), 101. https://doi.org/10.3390/fractalfract8020101
33. *Australian Energy Market Operator (AEMO), Aggregated price and demand data*, 2024.
34. *ASX Energy, Au electricity options*, 2024, Accessed: 2024:11-28.
35. *Open Electricity, Price and market data*, 2024, Accessed: 2024:11-28.
36. Á. Cartea, D. del Castillo-Negrete, Fractional diffusion models of option prices in markets with jumps, *Physica A*, **374** (2007), 749–763. https://doi.org/10.1016/j.physa.2006.08.071
37. A. Wyłomańska, J. Gajda, T. J. Kozubowski, Fractional dynamics in financial modeling: Theoretical development and applications, *Acta Phys. Pol. B*, **42** (2011), 1041–1052.

38. W. Sawangtong, P. Sawangtong, An analytical solution for the Caputo type generalized fractional evolution equation, *Alex. Eng. J.*, **61** (2022), 5475–5483. https://doi.org/10.1016/j.aej.2021.10.055

39. M. Caputo, M. Fabrizio, A new definition of fractional derivative without singular kernel, *Prog. Fract. Differ. Appl.*, **1** (2015), 73–85. http://dx.doi.org/10.12785/pfda/010201

40. J. Losada, J. J. Nieto, Properties of a new fractional derivative without singular kernel, *Prog. Fract. Differ. Appl.*, **1** (2015), 87–92. http://dx.doi.org/10.12785/pfda/010202

41. D. Applebaum, *Lévy processes and stochastic calculus*, Cambridge University Press, 2 Eds., 2009. https://doi.org/10.1017/CBO9780511809781

42. R. Cont, P. Tankov, *Financial modelling with jump processes*, Chapman and Hall/CRC, 2004. https://doi.org/10.1201/9780203485217

43. A. A. Kilbas, H. M. Srivastava, J. J. Trujillo, *Theory and applications of fractional differential equations*, **204** (2006), Elsevier.

44. R. Zacher, A de Giorgi-Nash type theorem for time fractional diffusion equations, *Math. Ann.*, **356** (2013), 99–146. https://doi.org/10.1007/s00208-012-0834-9

45. Y. Luchko, Maximum principle for the generalized time-fractional diffusion equation, *J. Math. Anal. Appl.*, **351** (2009), 218–223. https://doi.org/10.1016/j.jmaa.2008.10.018

46. R. Khalil, M. Al Horani, A. R. Yousef, M. Sababheh, A new definition of fractional derivative, *J. Comput. Appl. Math.*, **264** (2014), 65–70. https://doi.org/10.1016/j.cam.2014.01.002

AIMS Press